Virtual Reality over Wireless Networks: Quality-of-Service Model and Learning-Based Resource Management

Mingzhe Chen*, Walid Saad†, and Changchuan Yin*

*Beijing Laboratory of Advanced Information Network, Beijing University of Posts and Telecommunications, Beijing, China 100876, Emails: chenmingzhe@bupt.edu.cn, ccyin@ieee.org.

†Wireless@VT, Bradley Department of Electrical and Computer Engineering, Virginia Tech, Blacksburg, VA, USA, Email: walids@vt.edu.

arXiv:1703.04209v1 [cs.IT] 13 Mar 2017

Abstract

In this paper, the problem of resource management is studied for a network of wireless virtual reality (VR) users communicating over heterogeneous small cell networks (SCNs). In order to capture the VR users' quality-of-service (QoS) in SCNs, a novel VR model, based on multi-attribute utility theory, is proposed. This model jointly accounts for VR metrics such as tracking accuracy, processing delay, and transmission delay. In this model, the small base stations (SBSs) act as the VR control centers that collect the tracking information from VR users over the cellular uplink. Once this information is collected, the SBSs will then send the three dimensional images and accompanying surround stereo audio to the VR users over the downlink. Therefore, the resource allocation problem in VR wireless networks must jointly consider both the uplink and downlink. This problem is then formulated as a noncooperative game and a distributed algorithm based on the machine learning framework of echo state networks (ESNs) is proposed to find the solution of this game. The use of the proposed ESN algorithm enables the SBSs to predict the VR QoS of each SBS and guarantees the convergence to a mixed-strategy Nash equilibrium. The analytical result shows that each user's VR QoS jointly depends on both VR tracking accuracy and wireless resource allocation. Simulation results show that the proposed algorithm yields significant gains, in terms of total utility value of VR QoS, that reach up to 22% and 38.5%, respectively, compared to Q-learning and a baseline proportional fair algorithm. The results also show that the proposed algorithm has a faster convergence time than Q-learning and can guarantee low delays for VR services.

Index Terms— VR; mobility; resource allocation; echo state networks; learning.

A preliminary version of this work [1] was submitted to IEEE GLOBECOM

I. Introduction

The recent advances in storage, computing, big data analytics, and artificial intelligence will realize the much sought after vision of immersive technologies and user-centric applications such as virtual reality (VR) [2]. VR enables the users to experience and interact with virtual environments through a first-person view. For instance, every individual can use a VR device to walk around in a fully immersive world and travel to any destination, within the confines of their own home. However, if VR devices such as HTC Vive [3] rely on wired connections to a VR control center, such as computer, for processing the information (e.g., 3D image generation), then the users will be significantly restricted in the type of actions that they can take and VR applications that they can experience. In particular, when using wired networking solutions, VR users only can experience the VR applications within a very restricted area (limited by the wires) and, hence, they will not have the opportunity to use VR services anytime, anywhere. In order to enable pervasive and truly immersive VR applications, one can deploy wireless VR systems [4] that rely on reliable wireless connections, such as those provided by cellular networks. In particular, VR systems can use the wireless connectivity of emerging small cell networks (SCNs) [4] in which small cell base stations (SBSs) can act as the VR control centers that directly connect to the VR devices over wireless links and, consequently, the SBSs will collect the tracking* information from the VR devices and send the VR images to the VR devices over wireless cellular links. However, operating VR devices over wireless cellular networks such as SCNs faces many challenges [4] that include tracking accuracy, extremely low delay, high data rate, and effective image compression.

A. Related Work

The existing literature has studied a number of problems related to VR such as in [2], [4]–[9]. The authors in [2] and [4] discussed current and future trends of VR systems. However, these works are restricted to preliminary surveys that do not provide any mathematically rigorous modeling of VR over wireless networks. In [5], the authors propose a streaming scheme that delivers only the visible portion of a 360° video based on head movement prediction. In [6], an

*Here, tracking pertains to the fact that the immersive VR applications must continuously collect a very accurate localization of each user including the positions, orientation, and eye movement (i.e., gaze tracking).

algorithm for generating high-quality stereo panoramas is proposed. The authors in [7] proposed a real-time solution that uses a single commodity RGB-D camera to track hand manipulation. In [8], a reinforcement learning algorithm is proposed to guide a user's movement within VR immersive environment. The authors in [9] proposed an approach based on the three-dimensional (3D) heat maps to address the challenges such as delay and data rate that have to be considered in 3D environments. However, existing works such as in [2], [4]–[9] focus VR systems that are deployed over wired networks and, as such, these works do not capture any challenges of deploying VR over cellular networks. Moreover, most of these existing works [2], [4]–[9] only focus on the improvement of one VR quality-of-service (QoS) metric such as tracking method or improved generation of 3D images. Indeed, this prior art does not develop any VR-specific model that can capture all factors of VR QoS and, hence, these works fall short in addressing the challenges of optimizing VR QoS for wireless users.

Some recent works such as [10]–[14] have studied a number of ideas related to ultra-reliable and low-delay communication in wireless networks which can be relevant for VR applications. In [10], the authors proposed a rate-efficient power allocation strategy for delay-outage limited applications with constraints on energy consumption. In [11], a Halanay-type inequality based comparison principle is proposed to ensure the stability of stochastic delayed systems. The authors in [12] proposed a cross-layer transmission optimization approach for the so-called tactile Internet in which queueing delay, transmission delay, and packet loss/error probabilities are considered to characterize the reliability. In [13], the authors proposed a deployment strategy for machine-to-machine communications with the goal of meeting stringent delay and reliability requirements. The work in [14] introduced a novel frame structure to support multiuser spatial multiplexing, short latencies on the radio access interface and mobility. However, most of these existing works such as [10]–[14] focus on conventional machine type devices that transmit small data packets (e.g., sensors) and, hence, these works may not scale well to a VR network which typically requires ultra-reliable, low-delay, and high data rate transmission. Moreover, most of these existing works [10]–[14] which only focus on the transmission delay in wireless networks may not be applied to the VR network that requires not only low delay in transmission but also low delay during VR information processing and continuous user tracking.

B. Main Contributions

The main contribution of this paper is to introduce a novel framework for enabling wireless cellular networks to integrate VR applications and services. To our best knowledge, *this is the first work that develops a comprehensive framework for analyzing the performance of VR services over cellular networks.* This paper provides the following key contributions:

- We propose a novel VR model based on the tools of *multi-attribute utility theory* [15], to jointly capture the tracking accuracy, transmission delay and processing delay thus effectively quantifying the VR QoS for all users in a wireless VR network. In this VR model, the tracking information is transmitted from the VR users to the SBSs over the cellular uplink while the VR images are transmitted in the downlink from the SBSs to the users.
- For the considered VR applications over wireless, we analyze resource (subcarrier) allocation *jointly* over, the uplink and downlink. We formulate the problem as a noncooperative game in which the players are the SBSs. Each player seeks to find an optimal spectrum allocation scheme to optimize a utility function that captures the VR QoS.
- To solve this VR resource management game, we propose a learning algorithm based on echo state networks (ESNs) [16]–[18] that can predict the value of VR QoS that results from resource allocation and, hence, can reach a mixed-strategy Nash equilibrium (NE). The proposed ESN-based learning algorithm guarantees the convergence to a mixed-strategy NE. One unique feature of this algorithm is that, after training, it can use the stored ESN information to effectively find an optimal converging path to a mixed-strategy NE. Simulation result shows that the proposed algorithm significantly improves convergence time of up to 25% compared to Q-learning.
- We perform fundamental analysis on the gains and tradeoffs that stem from changing the number of uplink and downlink subcarriers for each user. This analytical result shows that, in order to improve the VR QoS of each user, we can improve the tracking system or increase the number of the subcarriers allocated to each user according to each user's specific state. Moreover, we prove the convergence of the proposed algorithm.
- Extensive simulations are used to assess the performance of the proposed framework. Simulation results show that the proposed algorithm can yield, respectively, 22% and 38.5%

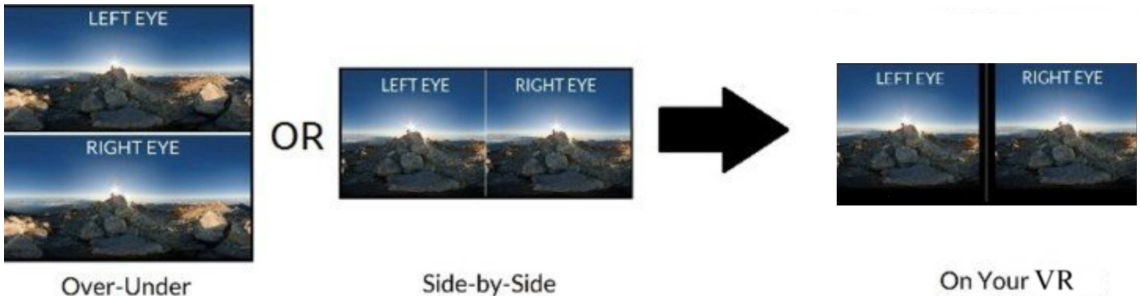

Fig. 1. The components of one VR view. Here, the 360° image for each eye is slightly different. These different images generate a 3D image for each VR user.

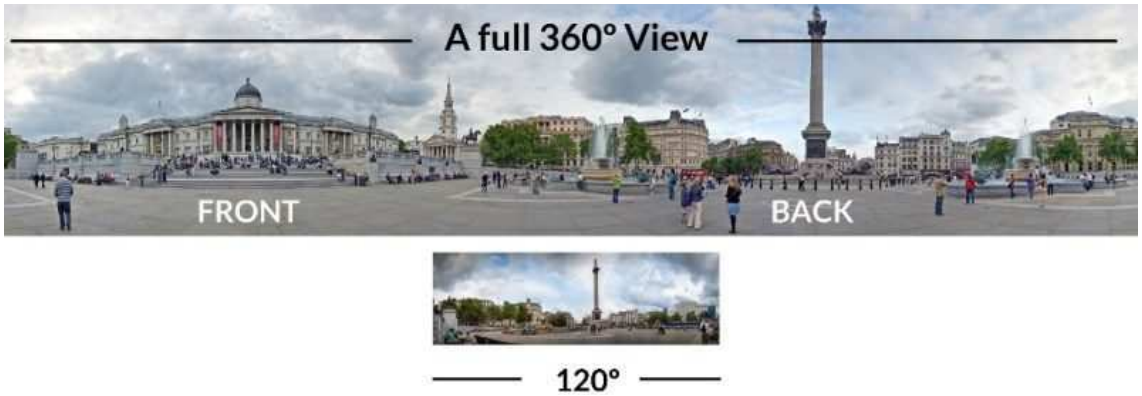

Fig. 2. The images taken from VR device and camera (the top 360° image is a VR image and the bottom 120° image is a mobile phone image). 360° image enables the VR users to have a vision without any dead spots and, hence, can be immersed in a surrounded virtual reality environment. Here, the dead spot corresponds to an area that the user cannot observe.

gains in terms of total utility value of VR QoS compared to Q-learning and proportional fair algorithm.

The rest of this paper is organized as follows. The system model and problem formulation are presented in Section II. The ESN-based resource allocation algorithm is proposed in Section III. In Section IV, numerical simulation results are presented and analyzed. Finally, conclusions are drawn in Section V.

II. System Model and Problem Formulation

Consider the downlink transmission of a cellular SCNs servicing a set $\mathcal{U}$ of V wireless VR users via a set $\mathcal{B}$ of B SBSs. Here, we focus on entertainment VR application such as watching immersive videos and playing immersive games [5]. In contrast to traditional mobile gaming and

TABLE I
LIST OF NOTATIONS

Notation	Description	Notation	Description
V	Number of users	$S^{\mathrm{d}}, S^{\mathrm{u}}$	Number of downlink and uplink subcarriers
B	Number of SBSs	$\mathcal{S}^{\mathrm{d}}, \mathcal{S}^{\mathrm{u}}$	Sets of downlink and uplink subcarriers
$\boldsymbol{W}_{\text{in}}$	Input weight matrix	D_{ij}^{T}	Transmission delay between user i and SBS j
P_B	Transmit power of SBSs	d_{ij}	Distance between user i and SBS j
$\mathcal{A}_j$	Set of SBS j's actions	c_{ij}	Data rate of user i associated with SBS j
$\boldsymbol{a}_j$	One action of SBS j	$\boldsymbol{s}_{ij}^{\mathrm{d}}, \boldsymbol{s}_{ij}^{\mathrm{u}}$	Subcarrier allocation vector
$\boldsymbol{a}_{ji}$	Action i of SBS j	$\boldsymbol{d}_j$	downlink subcarriers allocation of SBS j
$\boldsymbol{W}_{\text{out}}$	Output weight matrix	$\bar{u}_j$	Average utility function of SBS j
N_w	Number of reservoir units	$\hat{u}_j$	Utility function of SBS j
K_i	Tracking accuracy	γ_K	Maximal tracking inaccuracy
D_i	Total delay of user i	$\boldsymbol{v}_j$	Uplink subcarriers allocation of SBS j
$\boldsymbol{\chi}$	Vector of user's localization	$U_i\left(D_i, K_i\right)$	Total utility function of user i's VR QoS
λ	Learning rate	$U_i\left(D_i \mid K_i\right)$	Conditional utility function of user i's VR QoS
D_i^{P}	Processing delay of user i	V_j	Number of users associated with SBS j
$\boldsymbol{W}$	Reservoir weight matrix	$\lvert\mathcal{A}_j\rvert$	Number of SBS j's actions
$\boldsymbol{\mu}_j$	Reservoir state of SBS j	$\boldsymbol{a}_{-j}$	Actions of all SBSs other than SBS j

video streaming, the VR technology allows the users to be immersed in a virtual environment during which the users can experience a 3D and high-resolution 360° vision with 3D surround stereo, as shown in Figs. 1 and 2. Fig. 1 shows that immersive VR will provide a 360° panoramic image for each eye of a VR user. From Fig. 2, we can see that, compared to the 120° image, a 360° panoramic image enables the VR user have a surrounded vision without any dead spots. In this case, a VR image needs more pixels than a traditional two-dimensional image, and, hence, VR transmission will require more stringent requirements in terms of data rate (over 100 Mbps) [4], delay (less than 20 ms), and reliablility [19] than traditional multimedia services.

In our model, the SBSs adopt an orthogonal frequency division multiple access (OFDMA) technique and transmit over a set of $\mathcal{S}^{\mathrm{u}}$ of S^{u} uplink orthogonal subcarriers and a set of $\mathcal{S}^{\mathrm{d}}$ of S^{d} downlink orthogonal subcarriers, as shown in Fig. 3. The uplink subcarriers are used to transmit the data that is collected by the VR sensors placed at a VR user's headset or near the VR user while the downlink subcarriers are used to transmit the image displayed on each user's VR device. We first define the coverage of each SBS which is a circular area of radius r_B. We assume that each SBS only allocates subcarriers to the users located in its coverage range and each user will associate with its nearest SBS. We also assume that the subcarriers of each SBS

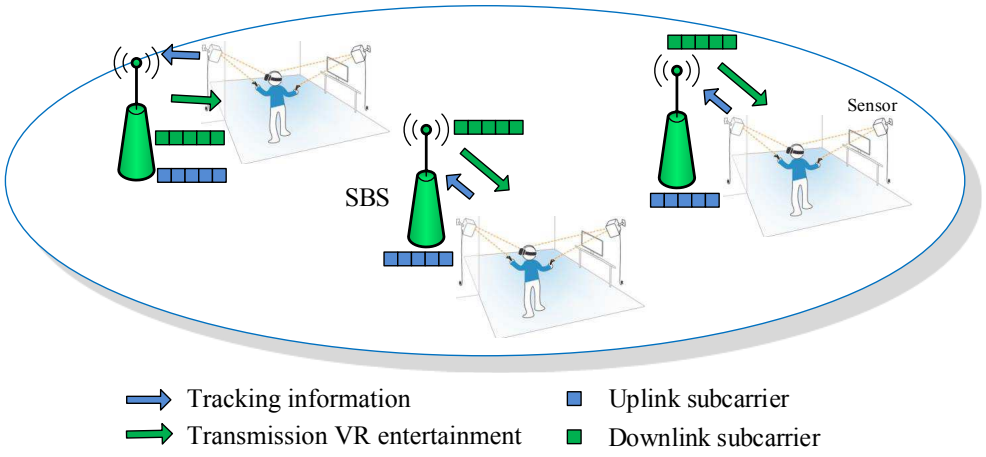

Fig. 3. A network of immersive VR application.

will all be allocated to the associated users. Table I provides a summary of the notations used hereinafter.

A. VR Model

In a VR model, we need to capture the VR transmission requirements such as high data rate, low delay, and accurate tracking. We consider delay and tracking accuracy as the main VR QoS metrics of interest. Based on the accurate localization of each user, the SBS can build the immersive and virtual environment for each user. Among the components of the VR QoS, a delay metric can be defined to capture two key VR service requirements: high data rate and low delay. Next, we will explicitly discuss all the components of the VR QoS metrics that will be accounted for.

1) Tracking Model: Within any VR QoS metric, tracking will consist of the position tracking and orientation tracking [5]. VR tracking directly affects the construction of the users' virtual environment. This is due to the fact that the SBSs need to use the user's localization information to construct the virtual environment. Hereinafter, we use the term "localization information" to represent the information related to the user's location and orientation. In this case, we use the localization of each user as the primary components of tracking [4]. The tracking vector of each user i can be given by $\boldsymbol{\chi}_i = [x_i, y_i, z_i, \phi_i, \varphi_i, \eta_i]$, where the vector $[x_i, y_i, z_i]$ represents the position of each VR user while the vector $[\phi_i, \varphi_i, \eta_i]$ represents the orientation of each user. Here, we need to note that the position and orientation of each user are determined by the SBS

via the information collected by the sensors. The tracking accuracy of each VR user, $K_i\left(\boldsymbol{s}_{ij}^{\mathrm{u}}\right)$, is given by [20]:

$$K_i\left(\boldsymbol{s}_{ij}^{\mathrm{u}}\right)=1-\frac{\left\|\boldsymbol{\chi}_i\left(\boldsymbol{s}_{ij}^{\mathrm{u}}\right)-\boldsymbol{\chi}_i^R\right\|}{\max\limits_{\boldsymbol{s}_{ij}^{\mathrm{u}}}\left\|\boldsymbol{\chi}_i\left(\boldsymbol{s}_{ij}^{\mathrm{u}}\right)-\boldsymbol{\chi}_i^R\right\|}, \tag{1}$$

where $\boldsymbol{\chi}_i\left(\boldsymbol{s}_{ij}^{\mathrm{u}}\right)$ is the localization determined by SBS j while $\boldsymbol{\chi}_i^R$ is the localization which can be obtained from the process of force feedback [21]. Here, force feedback represents the feedback that the users send to the SBSs whenever those users are not satisfied with the displayed VR image. Here, both localizations are transmitted via wireless links and, hence, the SBSs cannot receive the real localization of each user. In this case, we use the deviation between the localization determined by each SBS and the localization provided by user's force feedback to evaluate the tracking accuracy. The value of $\boldsymbol{\chi}_i\left(\boldsymbol{s}_{ij}^{\mathrm{u}}\right)$ depends on the uplink rate of each user. The increase of the uplink rate of each user enables the SBS to obtain more tracking information for a given user, and, hence, the SBSs can use more tracking information to determine the user's localization more accurately. Indeed, (1) is formulated based on normalized root mean square errors [20], which is a popular measure of the difference between two data sets. From (1), we can see that, as the number of subcarriers increases, the tracking error will decrease, which corresponds to the fact that whenever an SBS can obtain more tracking information about a given user, this SBS will be able to perform more accurate VR user tracking.

2) Delay: Next, we define the delay component that consists of the transmission delay and processing delay. The transmission delay of each user i can be given by:

$$D_{ij}^{\mathrm{T}}\left(\boldsymbol{s}_{ij}^{\mathrm{d}}\right)=\frac{L}{c_{ij}\left(\boldsymbol{s}_{ij}^{\mathrm{d}}\right)}, \tag{2}$$

where L is the size of VR image that each SBS needs to transmit to the associated users, $c_{ij}\left(\boldsymbol{s}_{ij}^{\mathrm{d}}\right)=\sum\limits_{k=1}^{S^{\mathrm{d}}}s_{ij,k}^{\mathrm{d}}B\log_2\left(1+\gamma_{ij}^k\right)$. Here, $\boldsymbol{s}_{ij}^{\mathrm{d}}=\left[s_{ij,1}^{\mathrm{d}},\ldots,s_{ij,S^{\mathrm{d}}}^{\mathrm{d}}\right]$ is the vector of subcarriers that SBS j allocates to user i with $s_{ij,k}^{\mathrm{d}}\in\{1,0\}$. $s_{ij,k}^{d}=1$ indicates that subcarrier k is allocated to user i. $\gamma_{ij}^k=\frac{P_B h_{ij}^k}{\sigma^2+\sum\limits_{l\in\mathcal{B}_k,l\neq j}P_B h_{il}^k}$ is the signal-to-interference-plus-noise ratio between user i and SBS j over subcarrier k with $\mathcal{B}_k$ being the set of the SBSs that use downlink subcarrier k. B is the bandwidth of each subcarrier, P_B is the transmit power of SBS j which is assumed to be equal for all SBSs, σ^2 is the variance of the Gaussian noise and $h_{ij}^k=g_{ij}^k p_{ij}^{-\beta}$ is the path loss between user i and SBS j over subcarrier with g_{ij}^k being the Rayleigh fading parameter, p_{ij} the distance between user i and SBS j, and β the path loss exponent. In the VR QoS, the *processing delay*

primarily stems from the tracking accuracy. Due to possibly inaccurate tracking, the SBS needs to adjust the virtual environment of each user. In this case, the SBS needs to spend additional time slots to re-construct the virtual environment and transmit it to the user. While no existing work has quantified this processing delay, we propose the following function:

$$D_i^{\mathrm{P}}\left(\boldsymbol{s}_{ij}^{\mathrm{u}}\right) = \upsilon \log_2\left(1 + K_i\left(\boldsymbol{s}_{ij}^{\mathrm{u}}\right)\right), \tag{3}$$

where υ is a scaling parameter that captures the relationship between the processing delay D_i^{P} and the tracking accuracy $K_i\left(\boldsymbol{s}_{ij}^{\mathrm{u}}\right)$. To our best knowledge, there is no existing work that considers the relationship between the tracking prediction and delay. From (3), we can see that inaccurate tracking will directly lead to an increased processing delay. That is due to the fact that each SBS must use additional time slots to re-construct and transmit the virtual environment to each VR user. However, as the inaccuracy increases, the processing delay will saturate at a given maximum value. This maximum value represents the time needed to retransmit the entire VR image to the user again. Hence, we propose (3) to capture this relationship. The total delay of each user i can hence be given by $D_i\left(\boldsymbol{s}_{ij}^{\mathrm{d}}, \boldsymbol{s}_{ij}^{\mathrm{u}}\right) = D_i^{\mathrm{P}}\left(\boldsymbol{s}_{ij}^{\mathrm{u}}\right) + D_i^{\mathrm{T}}\left(\boldsymbol{s}_{ij}^{\mathrm{d}}\right)$.

B. Utility Function Model

Next, we introduce a method based on the framework multi-attribute utility theory [15] to construct an appropriate utility function that can effectively capture the delay and tracking of VR QoS. Using multi-attribute utility theory, we can construct a total utility function that jointly considers the delay and tracking of the VR QoS. Conventional techniques for defining a utility function such as by directly summing up delay and tracking is only valid under the assumption that delay and tracking are independent and the values of the scaling constants are constrained. However, the utility function constructed by multi-attribute utility theory can assign to each delay and tracking components of the VR QoS a unique utility value without any constraints.

In order to construct the total utility function, we first define a conditional utility function for delay of VR QoS [15]. Here, the total utility function indicates that both tracking and delay will contribute to the utility value while, in the conditional utility function of delay, only delay contributes to the utility function and the tracking value is given. The conditional utility function can be used to formulate the total utility function which is similar to the formulation of joint probability function that uses conditional probability function. When the total utility function is

not easy to formulate, we can use the conditional utility function to formulate the total utility function. In our model, the total utility function of user i is given by $U_i\left(D_i\left(\boldsymbol{s}_{ij}^{\mathrm{d}}, \boldsymbol{s}_{ij}^{\mathrm{u}}\right), K_i\left(\boldsymbol{s}_{ij}^{\mathrm{u}}\right)\right)$, that jointly considers the delay and tracking of VR QoS. The conditional utility function of delay, $U_i\left(D_i\left(\boldsymbol{s}_{ij}^{\mathrm{d}}, \boldsymbol{s}_{ij}^{\mathrm{u}}\right)\middle|K_i\left(\boldsymbol{s}_{ij}^{\mathrm{u}}\right)\right)$, represents the total utility function given certain value of tracking accuracy. In our case, the tracking and delay are not independent and, hence, it is hard to formulate the total utility function directly. Therefore, we first formulate the conditional utility function of delay. As shown in [15], a suitable definition for a conditional utility of delay for user i can be given by:

$$U_i\left(D_i\left(\boldsymbol{s}_{ij}^{\mathrm{d}}, \boldsymbol{s}_{ij}^{\mathrm{u}}\right)\middle|K_i\left(\boldsymbol{s}_{ij}^{\mathrm{u}}\right)\right) = \begin{cases} \frac{D_{\max,i}\left(\boldsymbol{s}_{ij}^{\mathrm{u}}\right) - D_i\left(\boldsymbol{s}_{ij}^{\mathrm{d}}, \boldsymbol{s}_{ij}^{\mathrm{u}}\right)}{D_{\max,i}\left(\boldsymbol{s}_{ij}^{\mathrm{u}}\right) - \gamma_D}, & D_i\left(\boldsymbol{s}_{ij}^{\mathrm{d}}, \boldsymbol{s}_{ij}^{\mathrm{u}}\right) \geq \gamma_D, \\ \gamma_D, & D_i\left(\boldsymbol{s}_{ij}^{\mathrm{d}}, \boldsymbol{s}_{ij}^{\mathrm{u}}\right) < \gamma_D, \end{cases} \tag{4}$$

where γ_D is the maximal tolerable delay for each VR user (maximum supported by the VR system being used) and $D_{\max,i}\left(\boldsymbol{s}_{ij}^{\mathrm{u}}\right) = \max_{\boldsymbol{s}_{ij}^{\mathrm{d}}}\left(D_i\left(\boldsymbol{s}_{ij}^{\mathrm{d}}, \boldsymbol{s}_{ij}^{\mathrm{u}}\right)\right)$ is the maximum delay of VR user i given $\boldsymbol{s}_{ij}^{\mathrm{u}}$. Here, $U_i\big(D_{\max,i}\left(\boldsymbol{s}_{ij}^{\mathrm{u}}\right)\big|K_i\left(\boldsymbol{s}_{ij}^{\mathrm{u}}\right)\big) = 0$ and $U_i\big(\gamma_D\big|K_i\big(\boldsymbol{s}_{ij}^{\mathrm{u}}\big)\big) = 1$. Since delay and tracking are both dominant components, we can construct the total utility function, $U_i\left(D_i\left(\boldsymbol{s}_{ij}^{\mathrm{d}}, \boldsymbol{s}_{ij}^{\mathrm{u}}\right), K_i\left(\boldsymbol{s}_{ij}^{\mathrm{u}}\right)\right)$, that jointly considers the delay and tracking based on [15]. Here, a *dominant component* represents the component that will minimize the total utility function regardless of the value of other components. For VR QoS, delay and tracking are both dominant components. For example, the VR QoS will be minimized when the value of delay function is at a minimum regardless of the value of tracking accuracy. Dominant components such as delay and tracking will simplify the formulation of the total utility function [15]. Therefore, the total utility function of tracking and delay is [15]:

$$\begin{aligned} U_i\left(D_i\left(\boldsymbol{s}_{ij}^{\mathrm{d}}, \boldsymbol{s}_{ij}^{\mathrm{u}}\right), K_i\left(\boldsymbol{s}_{ij}^{\mathrm{u}}\right)\right) &= U_i\left(D_i\left(\boldsymbol{s}_{ij}^{\mathrm{d}}, \boldsymbol{s}_{ij}^{\mathrm{u}}\right)\middle|K_i\left(\boldsymbol{s}_{ij}^{\mathrm{u}}\right)\right) U_i\left(K_i\left(\boldsymbol{s}_{ij}^{\mathrm{u}}\right)\right), \\ &\overset{(a)}{=} \left(1 - \frac{\left\|\boldsymbol{\chi}_i\left(\boldsymbol{s}_{ij}^{\mathrm{u}}\right) - \boldsymbol{\chi}_i^R\right\|}{\max_{\boldsymbol{s}_{ij}^{\mathrm{u}}}\left\|\boldsymbol{\chi}_i\left(\boldsymbol{s}_{ij}^{\mathrm{u}}\right) - \boldsymbol{\chi}_i^R\right\|}\right) \frac{D_{\max,i}\left(\boldsymbol{s}_{ij}^{\mathrm{u}}\right) - D_i\left(\boldsymbol{s}_{ij}^{\mathrm{d}}, \boldsymbol{s}_{ij}^{\mathrm{u}}\right)}{D_{\max,i}\left(\boldsymbol{s}_{ij}^{\mathrm{u}}\right) - \gamma_D}. \end{aligned} \tag{5}$$

where (a) is obtained from the fact $U_i\left(K_i\left(\boldsymbol{s}_{ij}^{\mathrm{u}}\right)\right) = K_i\left(\boldsymbol{s}_{ij}^{\mathrm{u}}\right)$ and substituting (1) and (4) into (5). From (5), we can see that, the subcarriers allocated to user i for data transmission, $\boldsymbol{s}_{ij}^{\mathrm{d}}$, and the subcarriers allocated to user i for obtaining the tracking information, $\boldsymbol{s}_{ij}^{\mathrm{u}}$, jointly determine the value of the total utility function. Moreover, this total utility function can assign a unique value to each tracking and delay components of the VR QoS.

C. Problem Formulation

Given this system model, our goal is to develop an effective resource allocation scheme that allocates subcarriers in a way to maximize the VR QoS of all users. However, the maximization problem depends not only on the downlink subcarriers allocation but also on the uplink subcarriers allocation. Moreover, the VR QoS of each SBS depends not only on its own choice of the subcarriers allocation scheme but also on the remaining SBSs' schemes. In this regard, we formulate a noncooperative game $\mathcal{G} = \left[\mathcal{B}, \{\mathcal{A}_j\}_{j\in\mathcal{B}}, \{u_j\}_{j\in\mathcal{B}}\right]$. The SBSs in the game are the players. Each player j has a set $\mathcal{A}_j = \left\{\boldsymbol{a}_{j1}, \ldots, \boldsymbol{a}_{j|\mathcal{A}_j|}\right\}$ of $|\mathcal{A}_j|$ actions. In this game, each action of SBS j, $\boldsymbol{a}_j = (\boldsymbol{d}_j, \boldsymbol{v}_j)$ consists of: (i) downlink subcarriers allocation vector, $\boldsymbol{d}_j = \left[\boldsymbol{s}^{\mathrm{d}}_{1j}, \ldots, \boldsymbol{s}^{\mathrm{d}}_{V_j j}\right]$ and $\sum_{i=1}^{V_j} s^{d}_{ij,k} = 1$. Here, $\boldsymbol{s}^{\mathrm{d}}_{ij} = \left[s_{ij,1}, \ldots, s_{ij,S^{\mathrm{d}}}\right]$ represents the downlink subcarrier that SBS j allocates to user i and $s_{ij,k} \in \{1, 0\}$ with $s_{ij,k} = 1$ indicating that channel k is allocated to user i and $s_{ij,k} = 0$ otherwise. V_j is the number of all users in the coverage area of SBS j. (ii) uplink subcarriers allocation vector, $\boldsymbol{v}_j = \left[\boldsymbol{s}^{\mathrm{u}}_{1j}, \ldots, \boldsymbol{s}^{\mathrm{u}}_{V_j j}\right]$ and $\sum_{i=1}^{V_j} s^{\mathrm{u}}_{ij,k} = 1$. In our model, $\boldsymbol{a} = (\boldsymbol{a}_1, \boldsymbol{a}_2, \ldots, \boldsymbol{a}_B) \in \mathcal{A}$, represents the action profile of all players and $\mathcal{A} = \prod_{j\in\mathcal{B}} \mathcal{A}_j$.

To maximize the VR QoS of each user, the utility function of each SBS j can be given by:

$$u_j\left(\boldsymbol{a}_j, \boldsymbol{a}_{-j}\right) = \sum_{i=1}^{V_j} U_i\left(D_i\left(\boldsymbol{s}^{\mathrm{d}}_{ij}, \boldsymbol{s}^{\mathrm{u}}_{ij}\right), K_i\left(\boldsymbol{s}^{\mathrm{u}}_{ij}\right)\right), \tag{6}$$

where $\boldsymbol{a}_j \in \mathcal{A}_j$ is an action of SBS j and $\boldsymbol{a}_{-j}$ denotes the action profile of all SBSs other than SBS j. Let $\pi_{j,\boldsymbol{a}_i} = \lim_{T\to\infty} \frac{1}{T}\sum_{t=1}^{T} \mathbb{1}_{\{\boldsymbol{a}_j = \boldsymbol{a}_{ji}\}} = \Pr\left(\boldsymbol{a}_j = \boldsymbol{a}_{ji}\right)$ be the probability of SBS j using action $\boldsymbol{a}_{j,i}$ and, hence, $\boldsymbol{\pi}_j = \left[\pi_{j,\boldsymbol{a}_{j1}}, \ldots, \pi_{j,\boldsymbol{a}_{j|A_n|}}\right]$ is a probability distribution of SBS j. We assume that the VR transmission is analyzed during a period that consists of T time slots. Therefore, the average value of the utility function is:

$$\bar{u}_j\left(\boldsymbol{a}_j, \boldsymbol{a}_{-j}\right) = \lim_{T\to\infty} \frac{1}{T} \sum_{t=1}^{T} u_j\left(\boldsymbol{a}_j, \boldsymbol{a}_{-j}\right) = \sum_{\boldsymbol{a}\in\mathcal{A}} \left(u_j\left(\boldsymbol{a}_j, \boldsymbol{a}_{-j}\right) \prod_{j\in\mathcal{B}} \pi_{j,\boldsymbol{a}_j} \right). \tag{7}$$

Given the proposed model, our goal is to solve the proposed resource allocation game. A suitable solution for the studied game is the concept of the mixed-strategy Nash equilibrium, formally defined as follows [22]:

Definition 1. (mixed-strategy Nash Equilibrium): A mixed strategy profile $\boldsymbol{\pi}^* = (\boldsymbol{\pi}^*_1, \ldots, \boldsymbol{\pi}^*_B) = \left(\boldsymbol{\pi}^*_j, \boldsymbol{\pi}^*_{-j}\right)$ is a *mixed-strategy Nash equilibrium* if, $\forall j \in \mathcal{B}$ and $\boldsymbol{\pi}_j$, we have:

$$\bar{u}_j\left(\boldsymbol{\pi}^*_j, \boldsymbol{\pi}^*_{-j}\right) \geq \bar{u}_j\left(\boldsymbol{\pi}_j, \boldsymbol{\pi}^*_{-j}\right), \tag{8}$$

where $\bar{u}_j(\boldsymbol{\pi}_n, \boldsymbol{\pi}_{-n}) = \sum_{\boldsymbol{a}\in\mathcal{A}} u_j(\boldsymbol{a}) \prod_{n\in\mathcal{B}} \pi_{j,\boldsymbol{a}_j}$ is the expected utility of SBS j selecting the mixed strategy $\boldsymbol{\pi}_j$.

For our game, the mixed-strategy NE for the SBSs represents a solution of the game at which each SBS j can maximize the average VR QoS for its associated users, given the actions of its opponents.

III. Echo State Networks for Self-Organizing Resource Allocation

Next, we introduce a learning algorithm that can be used to solve the VR game and find its NE. In our game, since we consider both uplink and downlink subcarriers allocation, the number of actions will be much larger than conventional resource allocation scenarios that typically consider only the uplink or downlink subcarriers allocation. Therefore, as the number of actions significantly increases, using traditional game-theoretic algorithms such as fictitious play, each SBS may not be able to collect all information used to calculate the average utility function. Moreover, using such conventional game-theoretic and learning techniques, the SBSs will typically need to re-run the entire steps of the algorithm to reach a mixed-strategy NE as the states of the users and network vary. Hence, the delay during the convergence process of such algorithms may not be able to satisfy the QoS requirement of dynamic VR network. To satisfy the QoS requirement for the VR transmission of each SBS, we propose a learning algorithm based on the powerful framework of *echo state networks* (ESN) [23]. The proposed ESN-based learning algorithm enables each SBS to predict the value of VR QoS that results from each action and, hence, can reach a mixed-strategy NE without having to traverse all actions. Moreover, the proposed algorithm can store the past ESN information and, hence, can find an optimal convergence path from the initial state to a mixed-strategy NE. Next, we first introduce the components of an ESN-based learning algorithm. Then, we define the update process that the ESN-based learning algorithm uses to find the mixed-strategy NE.

A. ESN Components

An ESN-based learning algorithm consists of five components: a) agents, b) inputs, c) ESN model d), actions, and e) output. The specific components of the proposed ESN-based learning approach is thus defined as follows:

• *Agent*: The agents in our ESN are the SBSs in the set $\mathcal{B}$.

• *Actions:* Each action of SBS j, $\boldsymbol{a}_j$, jointly considers the uplink and downlink subcarriers, which is specified as follows:

$$\boldsymbol{a}_j = (\boldsymbol{d}_j, \boldsymbol{v}_j) = \left[\begin{array}{c} \boldsymbol{s}^{\mathrm{d}}_{1j} \cdots \boldsymbol{s}^{\mathrm{d}}_{V_j j}, \boldsymbol{s}^{\mathrm{u}}_{1j} \cdots \boldsymbol{s}^{\mathrm{u}}_{V_j j} \end{array} \right]^{\mathrm{T}}. \tag{9}$$

In order to guarantee that any action always has a non-zero probability to be chosen, the ε-greedy exploration [24] is adopted in the proposed algorithm. This mechanism is responsible for selecting the actions that each SBS will perform during the learning process while harmonizing the tradeoff between exploitation and exploration. Therefore, the probability with which SBS j chooses action i will be given by:

$$\Pr\left(\boldsymbol{a}_j\right) = \begin{cases} 1-\varepsilon+\frac{\varepsilon}{|\mathcal{A}_j|}, & \arg\max\limits_{\boldsymbol{a}_j \in \mathcal{A}_j} \hat{u}_{\tau,j}(\boldsymbol{a}_j), \\ \frac{\varepsilon}{|\mathcal{A}_j|}, & \text{otherwise}, \end{cases} \tag{10}$$

where $\hat{u}_{\tau,j}\left(\boldsymbol{a}_j\right) = \sum\limits_{\boldsymbol{a_{-j}} \in \mathcal{A}_{-j}} u_j\left(\boldsymbol{a}_j, \boldsymbol{a}_{-j}\right) \pi_{-j,\boldsymbol{a}_{-j}}$ is the expected utility of an SBS j with respect to the actions of its opponents, $\mathcal{A}_{-j} = \prod_{k \neq j, k \in \mathcal{B}} \mathcal{A}_k$ is the set of actions other than SBS j and $\pi_{-j,\boldsymbol{a}_{-j}} = \sum_{\boldsymbol{a}_j \in \mathcal{A}_j} \pi\left(\boldsymbol{a}_j, \boldsymbol{a}_{-j}\right)$ is the marginal probability distribution over the action set of SBS j. From (10), we can see that each SBS will assign the highest probability, $1-\varepsilon+\frac{\varepsilon}{|\mathcal{A}_j|}$, to the action that results in the maximum utility value, $\hat{u}_{\tau,j}$. For other actions, the SBS will assign the probability $\frac{\varepsilon}{|\mathcal{A}_j|}$. In this case, as each SBS maximizes the utility $\hat{u}_{\tau,j}$, the average utility $\bar{u}_j$ reaches maximum. In order to capture the gain that stems from the change of the number of subcarriers allocated to each user i, we state the following result:

Theorem 1. The gain of user i's VR QoS due to the change of the number of subcarriers allocated to user i can be given by:

i) The gain of user i that stems from the change of the number of uplink subcarriers allocated to user i, ΔU^{u}_i, can be given by:

$$\Delta U^{\mathrm{u}}_i = \left(D^{\mathrm{T}}_i\left(\boldsymbol{s}^{\mathrm{d}}_{\max}\right) - D^{\mathrm{T}}_i\left(\boldsymbol{s}^{\mathrm{d}}_{ij}\right)\right)\left(\frac{K_i\left(\boldsymbol{s}^{\mathrm{u}}_{ij}+\Delta\boldsymbol{s}^{\mathrm{u}}_{ij}\right)}{D^{\mathrm{T}}_i(\boldsymbol{s}^{\mathrm{d}}_{\max})+\upsilon\log_2\left(1+K_i\left(\boldsymbol{s}^{\mathrm{u}}_{ij}+\Delta\boldsymbol{s}^{\mathrm{u}}_{ij}\right)\right)-\gamma_{i,D}} - \frac{K_i\left(\boldsymbol{s}^{\mathrm{u}}_{ij}\right)}{D^{\mathrm{T}}_i\left(\boldsymbol{s}^{\mathrm{d}}_{\max}\right)+\upsilon\log_2\left(1+K_i\left(\boldsymbol{s}^{\mathrm{u}}_{ij}\right)\right)-\gamma_{i,D}}\right), \tag{11}$$

ii) The gain of VR user i that stems from the change of number of downlink subcarriers allocated

to user i, ΔU_i^{d}, can be given by:

$$\Delta U_i^{\mathrm{d}} = \begin{cases} \frac{K_i\left(\boldsymbol{s}_{ij}^{\mathrm{u}}\right)d_{ij}}{\left(D_{\max,i}\left(\boldsymbol{s}_{ij}^{\mathrm{u}}\right)-\gamma_{i,D}\right)c_{ij}\left(\boldsymbol{s}_{ij}^{\mathrm{d}}\right)}, & c_{ij}\left(\Delta \boldsymbol{s}_{ij}^{\mathrm{d}}\right) \gg c_{ij}\left(\boldsymbol{s}_{ij}^{\mathrm{d}}\right), \\ \frac{K_i\left(\boldsymbol{s}_{ij}^{\mathrm{u}}\right)d_{ij}c_{ij}\left(\Delta \boldsymbol{s}_{ij}^{\mathrm{d}}\right)}{\left(D_{\max,i}\left(\boldsymbol{s}_{ij}^{\mathrm{u}}\right)-\gamma_{i,D}\right)c_{ij}\left(\boldsymbol{s}_{ij}^{\mathrm{d}}\right)}, & c_{ij}\left(\Delta \boldsymbol{s}_{ij}^{\mathrm{d}}\right) \ll c_{ij}\left(\boldsymbol{s}_{ij}^{\mathrm{d}}\right), \\ \frac{K_i\left(\boldsymbol{s}_{ij}^{\mathrm{u}}\right)d_{ij}}{\left(D_{\max,i}\left(\boldsymbol{s}_{ij}^{\mathrm{u}}\right)-\gamma_{i,D}\right)} \times \frac{c_{ij}\left(\Delta \boldsymbol{s}_{ij}^{\mathrm{d}}\right)}{c_{ij}\left(\boldsymbol{s}_{ij}^{\mathrm{d}}\right)^2+c_{ij}\left(\boldsymbol{s}_{ij}^{\mathrm{d}}\right)c_{ij}\left(\Delta \boldsymbol{s}_{ij}^{\mathrm{d}}\right)}, & \text{else.} \end{cases} \tag{12}$$

Proof. For i), the gain that stems from increasing the number of uplink subcarriers allocated to user i, ΔU_i^{u}, can be calculated as follows:

$$\begin{aligned} &U_i\left(D_i\left(\boldsymbol{s}_{ij}^{\mathrm{d}}, \boldsymbol{s}_{ij}^{\mathrm{u}}+\Delta \boldsymbol{s}_{ij}^{\mathrm{u}}\right), K_i\left(\boldsymbol{s}_{ij}^{\mathrm{u}}+\Delta \boldsymbol{s}_{ij}^{\mathrm{u}}\right)\right) - U_i\left(D_i\left(\boldsymbol{s}_{ij}^{\mathrm{d}}, \boldsymbol{s}_{ij}^{\mathrm{u}}\right), K_i\left(\boldsymbol{s}_{ij}^{\mathrm{u}}\right)\right) \\ =&K_i\left(\boldsymbol{s}_{ij}^{\mathrm{u}}+\Delta \boldsymbol{s}_{ij}^{\mathrm{u}}\right) \times \frac{D_{\max,i}\left(\boldsymbol{s}_{ij}^{\mathrm{u}}+\Delta \boldsymbol{s}_{ij}^{\mathrm{u}}\right) - D_i\left(\boldsymbol{s}_{ij}^{\mathrm{d}}, \boldsymbol{s}_{ij}^{\mathrm{u}}+\Delta \boldsymbol{s}_{ij}^{\mathrm{u}}\right)}{D_{\max,i}\left(\boldsymbol{s}_{ij}^{\mathrm{u}}+\Delta \boldsymbol{s}_{ij}^{\mathrm{u}}\right)-\gamma_D} - K_i\left(\boldsymbol{s}_{ij}^{\mathrm{u}}\right) \times \frac{D_{\max,i}\left(\boldsymbol{s}_{ij}^{\mathrm{u}}\right) - D_i\left(\boldsymbol{s}_{ij}^{\mathrm{d}}, \boldsymbol{s}_{ij}^{\mathrm{u}}\right)}{D_{\max,i}\left(\boldsymbol{s}_{ij}^{\mathrm{u}}\right)-\gamma_D}, \\ =&\left(D_i^{\mathrm{T}}\left(\boldsymbol{s}_{\max}^{\mathrm{d}}\right)-D_i^{\mathrm{T}}\left(\boldsymbol{s}_{ij}^{\mathrm{d}}\right)\right)\left(\frac{K_i\left(\boldsymbol{s}_{ij}^{\mathrm{u}}+\Delta \boldsymbol{s}_{ij}^{\mathrm{u}}\right)}{D_i^{\mathrm{T}}\left(\boldsymbol{s}_{\max}^{\mathrm{d}}\right)+\upsilon \log_2\left(1+K_i\left(\boldsymbol{s}_{ij}^{\mathrm{u}}+\Delta \boldsymbol{s}_{ij}^{\mathrm{u}}\right)\right)-\gamma_{i,D}} - \frac{K_i\left(\boldsymbol{s}_{ij}^{\mathrm{u}}\right)}{D_i^{\mathrm{T}}\left(\boldsymbol{s}_{\max}^{\mathrm{d}}\right)+\upsilon \log_2\left(1+K_i\left(\boldsymbol{s}_{ij}^{\mathrm{u}}\right)\right)-\gamma_{i,D}}\right). \end{aligned} \tag{13}$$

Since function $K_i\left(x\right)$ is determined by the sensing method of VR system and there is no accurate model to capture the relationship between the tracking accuracy and subcarriers, (13) cannot be simplified.

For ii), the gain of changing the downlink subcarriers, ΔU_i^{d}, can be given by:

$$\begin{aligned} \Delta U_i^{\mathrm{d}} &= K_i\left(\boldsymbol{s}_{ij}^{\mathrm{u}}\right) \times \frac{D_i\left(\boldsymbol{s}_{ij}^{\mathrm{d}}, \boldsymbol{s}_{ij}^{\mathrm{u}}\right) - D_i\left(\boldsymbol{s}_{ij}^{\mathrm{d}}+\Delta \boldsymbol{s}_{ij}^{\mathrm{d}}, \boldsymbol{s}_{ij}^{\mathrm{u}}\right)}{D_{\max}\left(\boldsymbol{s}_{ij}^{\mathrm{u}}\right)-\gamma_{i,D}}, \\ &= K_i\left(\boldsymbol{s}_{ij}^{\mathrm{u}}\right) \times \frac{D_i^T\left(\boldsymbol{s}_{ij}^{\mathrm{d}}\right) - D_i^T\left(\boldsymbol{s}_{ij}^{\mathrm{d}}+\Delta s_{ij}^{\mathrm{d}}\right)}{D_{\max,i}\left(s_{ij}^{\mathrm{u}}\right)-\gamma_{i,D}}, \\ &= \frac{K_i\left(\boldsymbol{s}_{ij}^{\mathrm{u}}\right)}{D_{\max,i}\left(\boldsymbol{s}_{ij}^{\mathrm{u}}\right)-\gamma_{i,D}} \times \frac{d_{ij}c_{ij}\left(\Delta \boldsymbol{s}_{ij}^{\mathrm{d}}\right)}{c_{ij}\left(\boldsymbol{s}_{ij}^{\mathrm{d}}\right)c_{ij}\left(\boldsymbol{s}_{ij}^{\mathrm{d}}+\Delta \boldsymbol{s}_{ij}^{\mathrm{d}}\right)}, \\ &= \frac{K_i\left(\boldsymbol{s}_{ij}^{\mathrm{u}}\right)d_{ij}}{D_{\max,i}\left(\boldsymbol{s}_{ij}^{\mathrm{u}}\right)-\gamma_{i,D}} \times \frac{c_{ij}\left(\Delta \boldsymbol{s}_{ij}^{\mathrm{d}}\right)}{c_{ij}\left(\boldsymbol{s}_{ij}^{\mathrm{d}}\right)^2+c_{ij}\left(\boldsymbol{s}_{ij}^{\mathrm{d}}\right)c_{ij}\left(\Delta \boldsymbol{s}_{ij}^{\mathrm{d}}\right)}. \end{aligned} \tag{14}$$

Here, when $c_{ij}\left(\Delta \boldsymbol{s}_{ij}^{\mathrm{d}}\right) \gg c_{ij}\left(\boldsymbol{s}_{ij}^{\mathrm{d}}\right)$, $\frac{c_{ij}\left(\Delta \boldsymbol{s}_{ij}^{\mathrm{d}}\right)}{c_{ij}\left(\boldsymbol{s}_{ij}^{\mathrm{d}}\right)^2+c_{ij}\left(\boldsymbol{s}_{ij}^{\mathrm{d}}\right)c_{ij}\left(\Delta \boldsymbol{s}_{ij}^{\mathrm{d}}\right)} \approx \frac{1}{c_{ij}\left(\boldsymbol{s}_{ij}^{\mathrm{d}}\right)}$, and, consequently, $\Delta U_i^{\mathrm{d}} = \frac{K_i\left(\boldsymbol{s}_{ij}^{\mathrm{u}}\right)d_{ij}}{\left(D_{\max,i}\left(\boldsymbol{s}_{ij}^{\mathrm{u}}\right)-\gamma_{i,D}\right)c_{ij}\left(\boldsymbol{s}_{ij}^{\mathrm{d}}\right)}$. Moreover, as $c_{ij}\left(\Delta \boldsymbol{s}_{ij}^{\mathrm{d}}\right) \ll c_{ij}\left(\boldsymbol{s}_{ij}^{\mathrm{d}}\right)$, $\frac{c_{ij}\left(\Delta \boldsymbol{s}_{ij}^{\mathrm{d}}\right)}{c_{ij}\left(\boldsymbol{s}_{ij}^{\mathrm{d}}\right)^2+c_{ij}\left(\boldsymbol{s}_{ij}^{\mathrm{d}}\right)c_{ij}\left(\Delta \boldsymbol{s}_{ij}^{\mathrm{d}}\right)} \approx \frac{c_{ij}\left(\Delta \boldsymbol{s}_{ij}^{\mathrm{d}}\right)}{c_{ij}\left(\boldsymbol{s}_{ij}^{\mathrm{d}}\right)^2}$ and, consequently, $\Delta U_i^{\mathrm{d}} = \frac{K_i\left(\boldsymbol{s}_{ij}^{\mathrm{u}}\right)d_{ij}c_{ij}\left(\Delta \boldsymbol{s}_{ij}^{\mathrm{d}}\right)}{\left(D_{\max,i}\left(\boldsymbol{s}_{ij}^{\mathrm{u}}\right)-\gamma_{i,D}\right)c_{ij}\left(\boldsymbol{s}_{ij}^{\mathrm{d}}\right)}$. This completes the proof. □

From Theorem 1, we can see that the tracking accuracy, K_i, and the number of uplink subcarriers allocated to user i, will directly affect the VR QoS gain of user i. Therefore, in order to improve the VR QoS of each user, we can improve the tracking system or increase

the number of the subcarriers allocated to each user according to each user's specific state. Moreover, the gain due to the increasing number of downlink subcarriers depends on the values of data rates $c_{ij}\left(\Delta \boldsymbol{s}_{ij}^{\mathrm{d}}\right)$ and $c_{ij}\left(\boldsymbol{s}_{ij}^{\mathrm{d}}\right)$. Hence, the proposed learning algorithm needs to choose the optimal subcarriers allocation scheme to maximize the VR users' QoS.

• *Input:* The ESN-based learning algorithm takes input as a vector $\boldsymbol{x}_{\tau,j} = [x_1, \cdots, x_B]^{\mathrm{T}}$ where x_j represents the index of the probability distribution that SBS j uses at time τ. The vector $\boldsymbol{x}_{\tau,j}$ is then used to estimate the value of the utility value $\hat{\boldsymbol{u}}_j$ that captures the average VR QoS of SBS j, $\boldsymbol{y}_{\tau,j}$.

• *ESN Model:* An ESN model for each SBS j must be defined. This model is a learning architecture that can find the relationship between the input $\boldsymbol{x}_{t,j}$ and output $\boldsymbol{y}_{t,j}$, thus building the function between the SBS's probability distribution and the conditional utility value. Mathematically, the ESN model consists of the output weight matrix $\boldsymbol{W}_j^{\text{out}} \in \mathbb{R}^{|\mathcal{A}_j| \times N_w}$ and the dynamic reservoir containing the input weight matrix $\boldsymbol{W}_j^{\text{in}} \in \mathbb{R}^{N_w \times B}$, and the recurrent matrix $\boldsymbol{W}_j = \begin{bmatrix} w_{11} & 0 & 0 \\ 0 & \ddots & 0 \\ 0 & 0 & w_{N_w N_w} \end{bmatrix}$ with N_w being the number of the dynamic reservoir units. Here, the dynamic reservoir is used to store historical ESN information that includes input, reservoir state and output. Note that the historical ESN information can be used to find a fast converging process from the initial state to the mixed-strategy NE. Here, the number of actions for each SBS determines the output weight matrix and recurrent matrix of each ESN. Consequently, next, we derive the number of the actions of each SBS j, $|\mathcal{A}_j|$.

Proposition 1. Given the number of the downlink and uplink subcarriers, S^{d} and S^{u}, as well as the users located in the coverage of SBS j, V_j, the number of actions for each SBS j, $|\mathcal{A}_j|$, is given by:

$$|\mathcal{A}_j| = \begin{pmatrix} S^{\mathrm{d}} - 1 \\ |\mathcal{N}(V_j)| - 1 \end{pmatrix} \sum_{\boldsymbol{n} \in \mathcal{N}(V_j)} \prod_{i=1}^{V_j - 1} \begin{pmatrix} n_i \\ S^{\mathrm{u}} - \sum_{k=1}^{i-1} n_i \end{pmatrix}, \tag{15}$$

where $\begin{pmatrix} x \\ y \end{pmatrix} = \frac{x(x-1)\cdots(x-y+1)}{y(y-1)\cdots 1}$ and $\mathcal{N}(V_j) = \left\{ \boldsymbol{n} | \sum_{i=1}^{V_j} n_i = S^{\mathrm{d}}, n_i > 0 \right\}$ with $|\mathcal{N}(V_j)|$ being the number of elements in $\mathcal{N}(V_j)$.

TABLE II
ESN-BASED LEARNING ALGORITHM FOR SUBCARRIERS ALLOCATION

Inputs: Mixed strategy $\boldsymbol{x}_{\tau,j}$

Initialize: $\boldsymbol{W}_j^{\text{in}}$, $\boldsymbol{W}_j$, $\boldsymbol{W}_j^{\text{out}}$, and $\boldsymbol{y}_j = 0$.

for each time τ **do**.

(a) Estimate the value of the conditional utility function based on (17).

if $\tau == 1$

(b) Set the mixed strategy $\boldsymbol{\pi}_{\tau,j}$ uniformly.

else

(c) Set the mixed strategy $\boldsymbol{\pi}_{\tau,j}$ based on (10).

end if

(d) Broadcast the index of the mixed strategy to other SBSs.

(e) Receive the index of the mixed strategy as input $\boldsymbol{x}_{\tau,j}$.

(f) Perform action to calculate the actual value of conditional utility function.

(e) Update the dynamic reservoir state based on (16).

(g) Update the output weight matrix based on (18).

end for

Output: Prediction $\boldsymbol{y}_{\tau,j}$

Proof. See Appendix A. □

Based on Proposition 1, we can determine the matrix size of both $\boldsymbol{W}_j^{\text{out}}$ and $\boldsymbol{W}_j$. From Proposition 1, we can see that as the number of users increases, the number of actions increases. Moreover, the increasing number of subcarriers will also increase the number of actions. From Proposition 1, we can also see that the number of actions in the uplink is much larger than the number of actions in the downlink. This is due to the fact that in uplink, the interference of each user changes as the subcarriers allocated to each user vary. However, in downlink, the actions will not affect the interference of each user.

• *Output:* The output of the ESN-based learning algorithm at time τ is a vector of utility values $\boldsymbol{y}_{\tau,j} = \left[y_{\tau,j1}, y_{\tau,j2}, \ldots, y_{\tau,j|\mathcal{A}_j|}\right]$. Here, $y_{\tau,ji}$ represents the estimated value of utility $\hat{u}_{\tau,j}\left(\boldsymbol{a}_{ji}\right)$ due to action i of SBS j and, hence, the ESN output, $\boldsymbol{y}_j$, will converge to the utility $\hat{\boldsymbol{u}}_j = \left[\hat{u}_j\left(\boldsymbol{a}_{j1}\right), \ldots, \hat{u}_j\left(\boldsymbol{a}_{j|\mathcal{A}_j|}\right)\right]$.

B. ESN-Based Learning Algorithm for Subcarriers Allocation

Here, we present the proposed ESN-based learning algorithm to find a mixed strategy NE. The proposed learning algorithm can find an optimal convergence path from initial state to a

mixed-strategy NE. In this case, the proposed algorithm enables each SBS to reach a mixed-strategy NE traversing minimum number of strategies after training. In order to find the optimal convergence path, the proposed algorithm needs to store the past ESN information that consists of input, reservoir states, and output. The past ESN information from time 0 up until time τ is stored by the dynamic reservoir state $\boldsymbol{\mu}_{\tau,j}$. The dynamic reservoir state of each SBS j at time τ is given by:

$$\boldsymbol{\mu}_{\tau,j} = f\left(\boldsymbol{W}_j \boldsymbol{\mu}_{\tau-1,j} + \boldsymbol{W}_j^{\text{in}} \boldsymbol{x}_{\tau,j}\right), \tag{16}$$

where $f(x) = \frac{e^x - e^{-x}}{e^x + e^{-x}}$ is the tanh function. From (16), we can see that the dynamic reservoir state consists of the past dynamic reservoir states and the mixed strategy at time τ. In this case, the dynamic reservoir state actually stores the mixed strategy from time 0 to time τ. Based on the dynamic reservoir state, the proposed ESN algorithm will combine with the output weight matrix to estimate the value of conditional utility value. The estimation of the conditional utility value can be given by:

$$\boldsymbol{y}_{\tau,j} = \boldsymbol{W}_{\tau,j}^{\text{out}} \boldsymbol{\mu}_{\tau,j}, \tag{17}$$

where $\boldsymbol{W}_{\tau,j}^{\text{out}}$ is the output weight matrix at time slot τ. To enable the ESN to use reservoir state $\boldsymbol{\mu}_{\tau,j}$ to predict the conditional utility value, $\hat{u}_{\tau,ji}$, due to action $\boldsymbol{a}_{ji}$, we must train the output matrix $\boldsymbol{W}_j^{\text{out}}$ using a linear gradient descent approach, which can be given by:

$$\boldsymbol{W}_{\tau+1,ji}^{\text{out}} = \boldsymbol{W}_{\tau,ji}^{\text{out}} + \lambda \left(\hat{u}_{\tau,ji} - y_{\tau,ji}\left(\boldsymbol{x}_{\tau,j}^j, \boldsymbol{a}_{ji}\right)\right) \boldsymbol{\mu}_{\tau,j}^{\text{T}}, \tag{18}$$

where $\boldsymbol{W}_{\tau,ji}^{\text{out}}$ is row i of $\boldsymbol{W}_{\tau,j}^{\text{out}}$, λ is the learning rate, and $\hat{u}_{\tau,ji}$ is the actual utility value. Here, $\hat{u}_{\tau,ji}$ is estimated by the utility value resulting from the actions performed by each SBS during each time slot τ. Based on the above formulations, the distributed ESN-based learning algorithm performed by every SBS j is summarized in Table II.

C. Convergence of the ESN-Based Learning Algorithm

Now, we prove the convergence of the proposed ESN-based learning algorithm. Then, we prove that the proposed algorithm reaches a mixed-strategy NE.

Theorem 2. The proposed ESN-based learning algorithm converges to the conditional utility value, $\hat{\boldsymbol{u}}_j$, if any following conditions is satisfied:

i) λ is a constant and $\min_{\boldsymbol{W}_{ji}^{\text{in}},\boldsymbol{x}_{\tau,j},\boldsymbol{x}'_{\tau,j}} \boldsymbol{W}_{ji}^{\text{in}}\left(\boldsymbol{x}_{\tau,j}-\boldsymbol{x}'_{\tau',j}\right)\geq 2$, where $\boldsymbol{W}_{ji}^{\text{in}}$ represents the row i of $\boldsymbol{W}_{j}^{\text{in}}$.
ii) λ satisfies the Robbins-Monro conditions [23] ($\lambda(t)>0, \sum_{t=0}^{\infty}\lambda(t)=+\infty, \sum_{t=0}^{\infty}\lambda^2(t)<+\infty$).

Proof. See Appendix B. □

From Theorem 2, we can see that the convergence of the proposed algorithm depends on the values of the input weight matrix $\boldsymbol{W}_{ji}^{\text{in}}$ and the input $\boldsymbol{x}_{\tau,j}$. These values also affect the capacity of the ESN's memory. Here, the memory of a ESN represents the ability that an ESN can store the past ESN information. Therefore, the proposed algorithm of SBS j can converge to the conditional utility function $\hat{\boldsymbol{u}}_j$ by choosing appropriate $\boldsymbol{W}_{ji}^{\text{in}}$ and $\boldsymbol{x}_{\tau,j}$. Indeed, the proposed learning algorithm can converge to $\hat{\boldsymbol{u}}_j$ even when $\boldsymbol{W}_{ji}^{\text{in}}$ and $\boldsymbol{x}_{\tau,j}$ are generated randomly. This is due to the fact that the probability of $\boldsymbol{u}_{\tau,j}=\boldsymbol{u}'_{\tau',j}$ is particularly small since $\boldsymbol{u}_{\tau,j}$ has a larger number of elements (i.e. more than 500).

Following this proof of convergence, the fact that the algorithm will reach a mixed NE follows directly from [25, Theorem 3].

Corollary 1. The ESN-based learning algorithm of each SBS j converges to a mixed-strategy Nash equilibrium, with the mixed strategy probability $\boldsymbol{\pi}_j^*$, $\forall j\in\mathcal{B}$.

Here, based on (10), each SBS will assign the highest probability to the action that results in the maximum value of $\hat{u}_{j,\max}=\max_{\boldsymbol{a}_j\in\mathcal{A}_j}\hat{u}_{\tau,j}(\boldsymbol{a}_j)$. Therefore, when each SBS j reaches the optimal mixed strategy $\boldsymbol{\pi}_j^*$ and the ESN reaches the maximal utility $\hat{\boldsymbol{u}}_j$, the maximum value of the average utility $\bar{u}_j$ can be given by $\left(1-\varepsilon+\frac{\varepsilon}{|\mathcal{A}_j|}\right)\hat{u}_{j,\max}$.

D. Implementation and Complexity

Next, the implementation and complexity of the proposed ESN-based learning algorithm are analyzed. The proposed algorithm can be implemented in a distributed way. At the initial state, the reservoir and output of the ESN is zero. During each iteration, the output and reservoir of ESN will be updated based on (16)-(17). Based on the ESN's output, each SBS will update its mixed strategy and broadcast the index of this mixed strategy to other SBSs. This interaction between SBSs is independent of the network size and, hence, incurs no notable overhead. In our model, the localization information is collected from two methods: 1) each SBS's own computation and 2) force feedback. The wireless transmission may affect the accuracy of both the localization

information collected from these methods. However, the localization of each user determined by the SBSs depends, not only on the quality of wireless transmission, but also on the uplink data rate and accuracy of VR sensor system. In this case, both the localization information collected from two methods may not be completely accurate, thus justifying the need for multiple forms of tracking. Hence, we consider the difference between the localization information determined by the SBSs and the information provided by user's force feedback in (1). We consider that the tracking is not accurate when the deviation is large and the tracking is accurate otherwise. This is due to the fact that a large deviation indicates that one of the two generated localization information is potentially inaccurate and, hence, the SBSs must check/improve the tracking system. As the input (index of mixed strategy) of ESN leads to a maximum output (utility value $\hat{\boldsymbol{u}}$), the ESN will be stable at this state and reaches a mixed-strategy NE.

The purpose of the proposed game is to find the optimal mixed strategy for each SBS. Hence, the complexity of the proposed algorithm depends on the number of mixed strategy. Based on (10), we can see that the number of mixed strategy is equal to the number of actions. Since the worst-case for each SBS is to traverse all actions, the worst case complexity of the proposed algorithm is $O(|\mathcal{A}_1| \times \cdots \times |\mathcal{A}_B|)$. However, the worst-case complexity pertains to a rather unlikely scenario in which all SBSs choose their optimal probability strategies after they traverse all other mixed strategies and, hence, the probability of the occurrence of the worst-case complexity is $\left(1-\frac{\varepsilon}{|\mathcal{A}_1|}\right)^{|\mathcal{A}_1|-1}\times\cdots\times\left(1-\frac{\varepsilon}{|\mathcal{A}_B|}\right)^{|\mathcal{A}_B|-1}$ [†]. Therefore, the proposed algorithm will converge faster than the worst-case with probability $1-\left(1-\frac{\varepsilon}{|\mathcal{A}_1|}\right)^{|\mathcal{A}_1|-1}\times\cdots\times\left(1-\frac{\varepsilon}{|\mathcal{A}_B|}\right)^{|\mathcal{A}_B|-1}$. Moreover, as the number of SBSs increases, based on Proposition 1, the number of actions for each SBS significantly decreases. In this case, the worst-case complexity of the proposed algorithm will also decrease. In addition, since the proposed ESN algorithm can at most store N_w information related to ESN [26], the ESN-based learning algorithm can use this past information to predict the value of utility $\hat{\boldsymbol{u}}_j$ and, hence, each SBS can obtain the VR QoS of each SBS without implementing the actions, which will also decrease the complexity of the proposed algorithm. During the convergence process, the proposed algorithm needs to harmonize the

[†] Based on (10), for each SBS, the probability that the optimal action is not selected at each iteration is $\left(1-\frac{\varepsilon}{|\mathcal{A}_j|}\right)$ and hence, the probability that the optimal action is selected at the last iteration is $\left(1-\frac{\varepsilon}{|\mathcal{A}_j|}\right)^{|\mathcal{A}_j|-1}$. Therefore, the probability of all SBSs select their optimal action at last iteration is $\left(1-\frac{\varepsilon}{|\mathcal{A}_1|}\right)^{|\mathcal{A}_1|-1}\times\cdots\times\left(1-\frac{\varepsilon}{|\mathcal{A}_B|}\right)^{|\mathcal{A}_B|-1}$.

tradeoff between the exploration and exploitation. Here, exploration is the process using which each SBS can adopt actions other than the current optimal action to find a better solution. Exploitation refers to the case in which each SBS will use the current optimal action at this iteration. This tradeoff is controlled by the ε-greedy exploration specificed in (10). If we increase the probability of exploration, the proposed algorithm will use more actions and, hence, the iteration that the proposed algorithm requires to reach a mixed-strategy NE decreases. However, the increasing probability of the exploration may reduce the VR QoS of each user when the selected action is worse than the current optimal action.

IV. Simulation Results

For our simulations, we consider an SCN deployed within a circular area with radius $r = 100$ m. $U = 25$ users and $B = 4$ SBSs are uniformly distributed in this SCN area. The Oculus VR device is considered in our simulations and, hence, the number of pixels for a panoramic image is 1920×1080 and each pixel is stored in 32 bits [27]. The flashed rate which represents the update rate of a VR image, is 60 images per second and the factor of compression is 300 [4]. Since two panoramic images consist of one VR image (one panoramic image per eye), the rate requirement of VR transmission will be 25.32 Mbit/s[‡]. The bandwidth of each subcarrier is set to 2 MHz [28]. The detailed parameters are listed in Table III. For comparison purposes, we use two baselines: a) Proportional fair algorithm [29] and b) Q-learning algorithm in [30]. Note that, in order to compare with the proportional fair algorithm, all SBSs choose the action with highest probability among the mixed strategy when the proposed algorithm reaches a mixed-strategy NE. This is used for all results in which we compare to proportional fair. Here, the data of users' localizations are measured from an actual wired Oculus VR devices and the wireless transmission is simulated, in order to compute the tracking accuracy. All statistical results are averaged over a large number of independent runs.

Fig. 4 shows how each user's VR QoS utility varies as the tracking and delay utilities change. In Fig. 4, different colors indicate different total VR QoS utilities. From Fig. 4, we can see that when the delay (tracking) utility is 0, the total VR QoS utility will be 0 regardless of the tracking (delay) value. This highlights the fact that both tracking accuracy and delay will affect

[‡]Here, for each second, each SBS needs to transmit $1920 \times 1080 \times 32 \times 60 \times 2 = 7,962,624,000$ bits $= 7593.75$ Mbits to each user. Since the factor of compression is 300, the rate requirement is $7593.75/300 = 25.3125$ Mbit/s.

TABLE III
SYSTEM PARAMETERS

Parameter	Value	Parameter	Value
F	1000	P_B	20 dBm
B	4	S^{u}, S^{d}	5, 5
N_w	1000	σ^2	-95 dBm
N_v	6	λ	0.03
υ	5	r_B	25 m

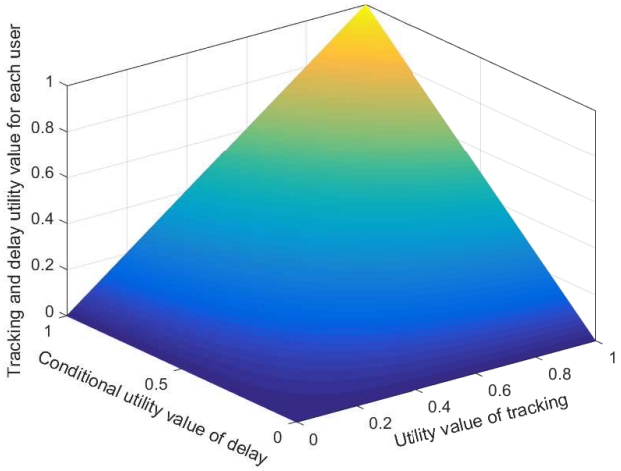

Fig. 4. Total VR QoS utility of each user vs. the tracking and delay utilities. Here, total VR QoS utility refers to (5).

the VR QoS. In Fig. 4, we can also see that only when both tracking and delay utilities are 1, the total VR QoS utility is maximized. This is due to the fact that the multi-attribute utility theory model assigns to each tracking and delay components of the VR QoS a unique value. Based on these observations, it is clear that, the proposed total utility function can effectively capture the VR QoS.

In Fig. 5, we show how each user's total VR QoS utility changes function of the tracking accuracy and the bandwidth of each downlink and uplink subcarrier. Fig. 5 uses the same color legends as Fig. 4. For example, in both Figs. 4 and 5, the yellow regions capture the case in which the total VR QoS utility is maximized. From Fig. 5, we can see that when the bandwidth of downlink (uplink) subcarrier is 0, the total VR QoS utility is 0 regardless of the bandwidth of uplink (downlink) subcarrier. This is due to the fact that the VR QoS depends on both delay and tracking. This corresponds to a scenario in which SBS j has enough downlink bandwidth to send a VR image to the user while the tracking information is inaccurate. In this case, SBS j

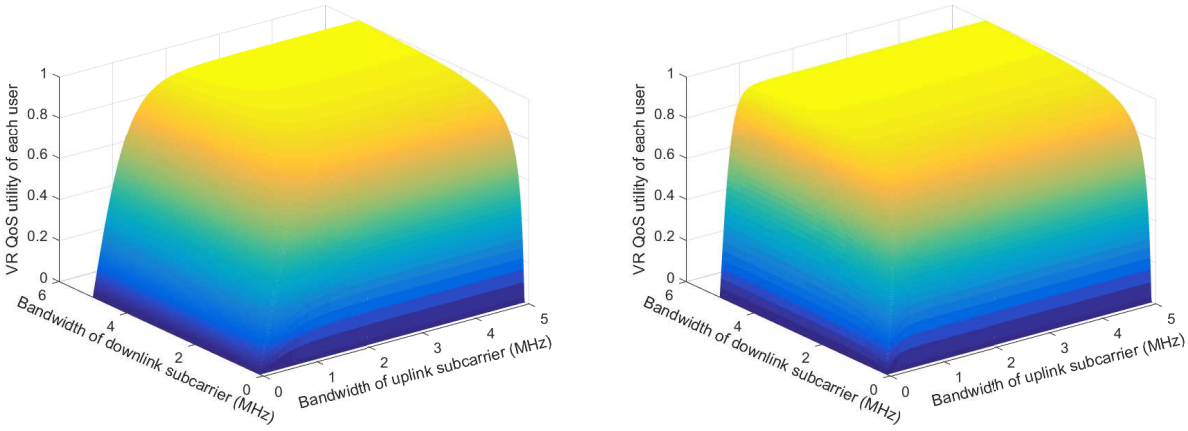
VR QoS utility of each user
Bandwidth of downlink subcarrier (MHz)
Bandwidth of uplink subcarrier (MHz)
VR QoS utility of each user
Bandwidth of downlink subcarrier (MHz)
Bandwidth of uplink subcarrier (MHz)

(a) (b)

Fig. 5. Total VR QoS utility of each user vs. the bandwidth of downlink and uplink subcarriers and tracking accuracy. Here, total VR QoS utility refers to (5). The tracking accuracy in Fig. 5(b) is more accurate than the tracking accuracy in Fig. 5(a).

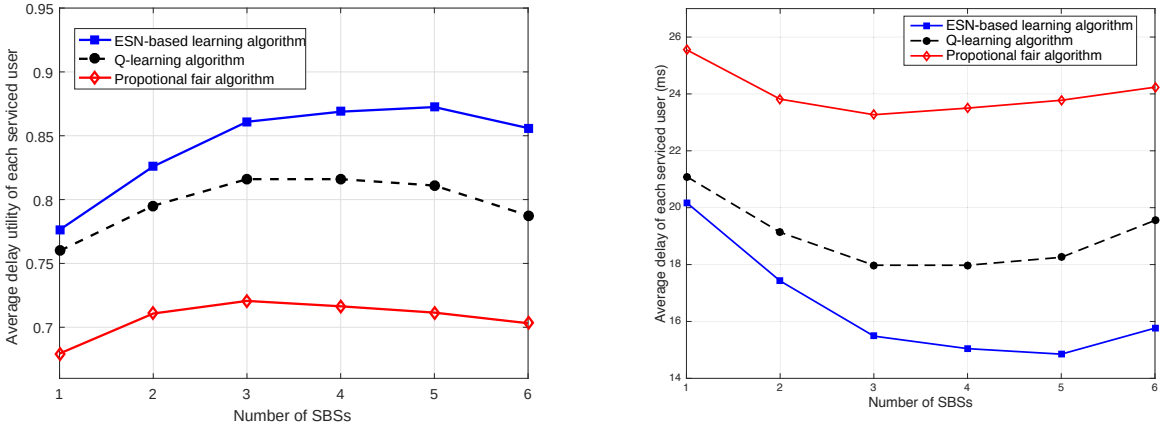

(a) Average delay utility of each serviced users (b) Average delay of each serviced users

Fig. 6. Delay for each serviced user vs. the number of SBSs.

cannot construct the accurate VR image due to the inaccuracy of user's localization and, hence, the VR QoS of this user will be 0. Fig. 5(a) also shows that when the bandwidth of uplink subcarrier is over 2 MHz and the bandwidth of downlink subcarrier is over 4 MHz, the total VR QoS utility will be maximized. From Figs. 5(a) and 5(b), we can see that, as the tracking accuracy increases, the uplink subcarrier bandwidth that each user needs to maximize the VR QoS decreases. This stems from the fact that tracking accuracy affects the processing delay. This verifies the result of Theorem 1 which showed both tracking accuracy and subcarriers allocation affect the users' VR QoS.

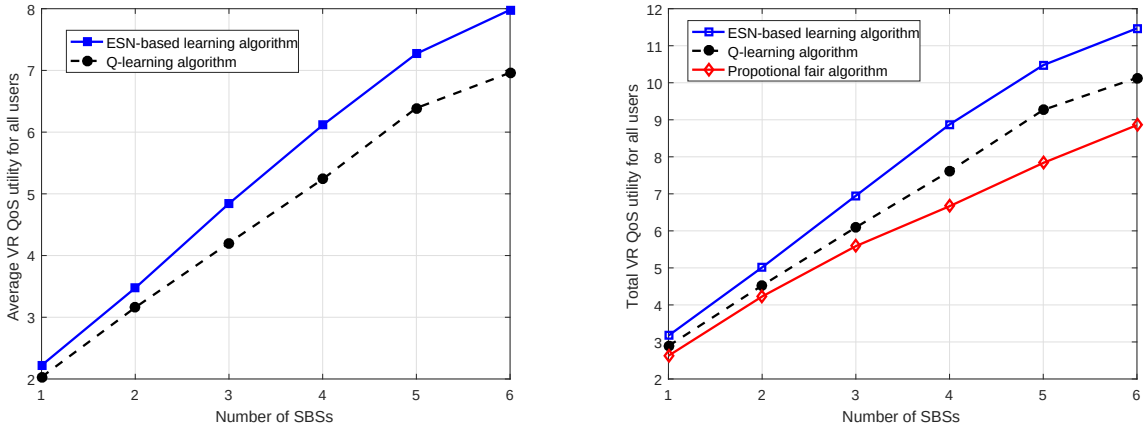

(a) Average total VR QoS utility for all users

(b) Total VR QoS utility for all users

Fig. 7. VR QoS for all users vs. the number of SBSs. Here, total VR QoS utility refers to (6)

In Fig. 6, we show how the average delay utility for each servicing user varies as the number of SBSs increases. From Figs. 6(a) and 6(b), we can see that as the number of SBSs increases, both the average delay utility and transmission delay for each serviced user increases then decreases. This is due to the fact that as the number of SBSs increases, the number of users located in each SBS's coverage decreases and, hence, the average delay utility increases. However, as the number of SBSs keeps increasing, the average delay utility decreases. This stems from the fact that the interference from the SBSs to the users increases as the number of SBSs continues to increase. Fig. 6(b) also shows that the proposed algorithm achieves up to 18.6% gain in terms of average delay compared to the Q-learning algorithm for the case with 6 SBSs. In Fig. 6(b), we can also see that the proposed ESN-based learning algorithm enables the wireless VR transmission to meet typical delay requirement of VR applications (typically 20 ms [31]). These gains stem from the fact that the proposed algorithm use the past ESN information stored at the ESN model to find a better solution for the proposed game.

Fig. 7 shows how the VR QoS for all users changes as the number of SBSs varies. From Figs. 7(a) and 7(b), we can see that both total utility values and average total utility values (at the mixed-strategy NE) of all considered algorithms increase as the number of SBSs increases. This is due to the fact that, as the number of SBSs increases, the number of users located within the coverage of each SBS increases and the distances from the SBSs to their associated users decrease. Fig. 7(a) shows that the proposed algorithm can yield up to of 16.1% gain in terms of the average of total VR QoS utility compared to the Q-learning for the case with 5 SBSs. In Fig.

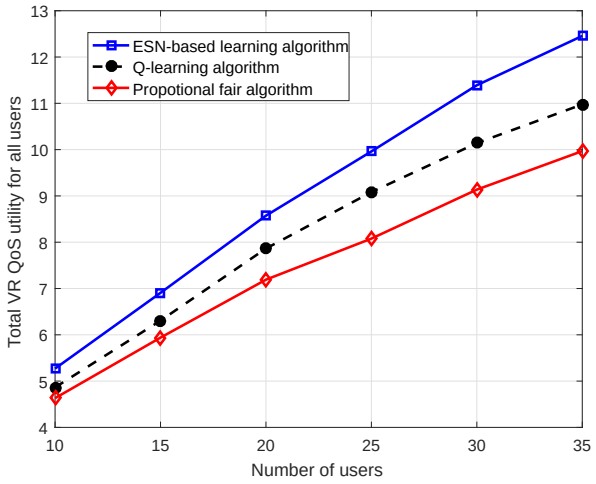

Fig. 8. The total VR QoS utility for all users vs. total number of users. Here, total VR QoS utility refers to (6)

7(b), we can also see that the proposed ESN-based learning algorithm achieves, respectively, up to 22% and 38.5% improvements in terms of the total utility value compared to Q-learning and proportional fair algorithms for the case with 4 SBSs. Clearly, these gains are due to the fact that the proposed ESN algorithm can store the past ESN information and use this information to build the relationship between the input and output. In this case, the proposed learning algorithm can predict the output (conditional utility value) and, hence, find a better solution for allocating resources.

In Fig. 8, we show how the total utility value of VR QoS for all users changes as the total number of users varies. From Fig. 8, we can see that as the number of users increases, the total utility values of all considered algorithms increase. This is due to the fact that, in all algorithms, each SBS has a limited coverage area and, hence, the number of users located in each SBS's coverage increases with the network size. Moreover, since each SBS has a limited number of subcarriers, the number of users that can associate with each SBS is also bounded. In particular, as the number of users located within the coverage of a given SBS exceeds the maximal number of users that each SBS can provide service, the SBS will only service the users that can maximize the total utility value. The VR QoS of the remaining users will be 0. In this case, the total utility value will also increase with the number of the users. From Fig. 8, we can also see that the proposed algorithm achieves, respectively, up to 13.6% and 25% gains in terms of the total utility value of VR QoS compared to Q-learning and proportional fair algorithms for the case with 35 users. This is due to the fact the proposed ESN algorithm can predict the utility value resulting

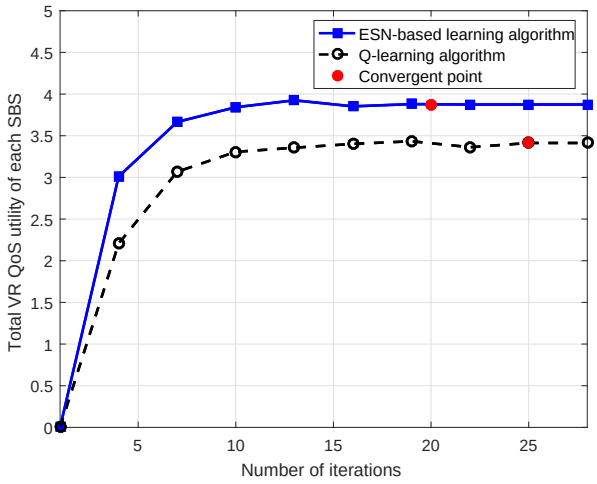

Fig. 9. Convergence of the proposed algorithm and Q-learning. Here, total VR QoS utility refers to (6)

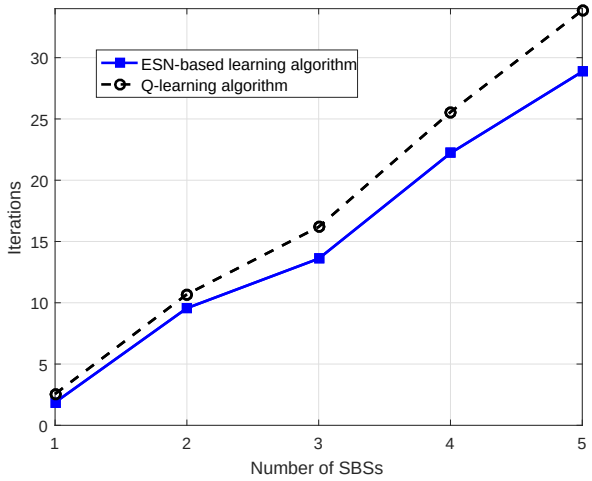

Fig. 10. The convergence time as a function of the number of SBSs.

from different actions and, hence, can find the optimal action to optimize the users' VR QoS.

Fig. 9 shows the number of iterations needed till convergence for both the proposed ESN-based learning approach and Q-learning. In this figure, we can see that, as time elapses, the total VR QoS utilities for both the proposed algorithm and Q-learning increase until convergence to their final values. Fig. 9 also shows that the proposed algorithm needs 20 iterations to reach convergence while Q-learning needs 25 iterations to reach convergence. Hence, the proposed algorithm achieves 25% gain in terms of the number of the iterations needed to reach convergence compared to Q-learning. This is due to the fact that the ESN in the proposed algorithm can store the SBSs' action strategies and its corresponding total utility values.

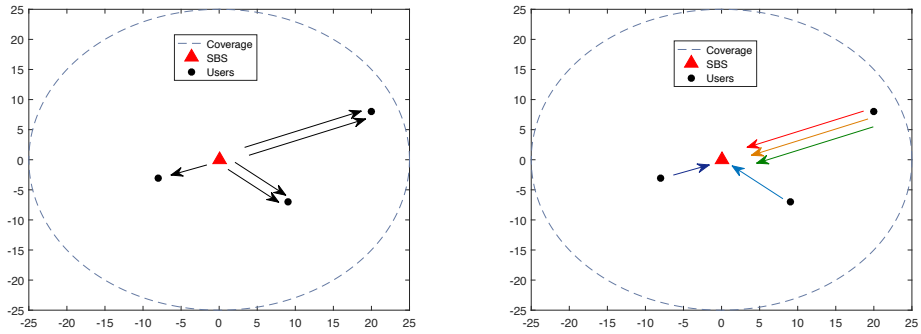

(a) Optimal action of the ESN-based algorithm for the users over downlink and uplink

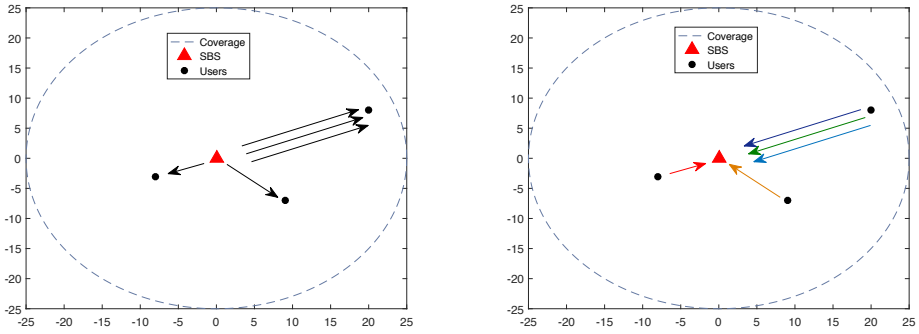

(b) Optimal action of proportional fair algorithm for the users over downlink and uplink

Fig. 11. Optimal actions resulting from the different algorithms (Each black arrow represents the downlink subcarrier while each color arrow represents an uplink subcarrier).

In Fig. 10, we show how the convergence time changes as the number of SBSs varies. In this figure, we can see that as the number of the SBSs increases, the convergence time of both algorithms increases. Indeed, as the number of SBSs increases, the proposed ESN algorithm will require more time to accurately calculate the VR QoS utility. From Fig. 10, we can also see that as the number of SBSs increases, the difference in the convergence time between the proposed algorithm and Q-learning increases. This stems from the fact that as the number of SBSs increases, the number of actions for each SBS decreases and, hence, the number of output weight matrix used to predict the VR QoS utility for each action decreases.

Fig. 11 shows the optimal actions resulting from the proposed ESN-based learning algorithm and proportional fair algorithm. Here, each color arrow represents a unique uplink subcarrier. From Figs. 11(a) and 11(b), we can see that, in the downlink subcarrier allocation, the proportional fair algorithm allocates most of the downlink subcarriers to the user located farthest to the

SBS while the proposed learning algorithm allocates only two subcarriers to the farthest user. This is due to the fact that the proportional fair algorithm only considers the users' subcarriers demands while the proposed learning algorithm considers how to maximize the total utility values of VR QoS for all associated users. Figs. 11(a) and 11(b) also show that, both the proposed ESN-based learning algorithm and proportional fair algorithm allocate three subcarriers to the farthest user. However, the uplink subcarriers allocated to each user are different. This is due to the fact that, in uplink, the proportional fair algorithm only considers the users' subcarrier demands while ignoring the uplink interference pertaining to the allocation of uplink subcarriers. In this case, the interference of users in uplink will significantly decrease the total VR QoS utility for each user. Note that, since each SBS allocates their all downlink and uplink subcarriers to its associated users, the interference of the users in downlink will not change as the actions vary while the interference of users in uplink depends on the actions.

V. Conclusion

In this paper, we have developed a novel multi-attribute utility theory based VR model that can capture the tracking and delay components of VR QoS. Based on this model, we have proposed a novel resource allocation framework for optimizing the VR QoS for all users. We have formulated the problem as a noncooperative game between the SBSs that seeks to maximize the average VR QoS utilities for all users. To solve this problem, we have developed a novel algorithm based on the machine learning tools of echo state networks. The proposed algorithm enables each SBS to decide on its actions autonomously according to the users' and networks' network states. Moreover, the proposed learning algorithm only needs to update the mixed strategy during the training process and, hence, can quickly converge to a mixed-strategy NE. Simulation results have shown that the proposed VR model can capture the VR QoS in wireless networks. Simulation results also show that the proposed approach yields significant performance gains in terms of total VR QoS utilities for all users compared to conventional approaches.

Appendix

A. *Proof of Proposition* 1

To prove Proposition 1, we first need to prove that the number of actions for the users over the downlink is $\begin{pmatrix} S^{\mathrm{d}}-1 \\ |\mathcal{N}(V_j)|-1 \end{pmatrix}$. Since the SBSs will allocate all downlink subcarriers to their

associated users, the interference from each SBS to its associated users is unchanged when the actions change. For example, the interference when SBS j allocates subcarrier 1 to user i is the same as the interference when SBS j allocates subcarrier 2 to user i. Therefore, we only need to consider the number of downlink subcarriers allocated to each user and, consequently, the number of actions for the users over the downlink is $\begin{pmatrix} S^{\mathrm{d}}-1 \\ |\mathcal{N}(V_j)|-1 \end{pmatrix}$. Then, we need to prove that the number of actions for the users over the uplink is $\sum\limits_{\boldsymbol{n}\in\mathcal{N}(V_j)}\prod\limits_{i=1}^{V_j-1}\begin{pmatrix} n_i \\ S^{\mathrm{u}}-\sum_{k=1}^{i-1}n_i \end{pmatrix}$. For each vector $\boldsymbol{n}$, SBS j has $\begin{pmatrix} n_1 \\ S^{\mathrm{u}} \end{pmatrix}$ actions to allocate the subcarriers to the first user. Based on the subcarriers allocated to the first user, SBS j will have $\begin{pmatrix} n_2 \\ S^{\mathrm{u}}-n_1 \end{pmatrix}$ actions to allocate the subcarriers to the second user. For other associated users, the number of actions can be derived using a similar method as the method of the second user. Therefore, the number of actions for the users over uplink is $\sum\limits_{\boldsymbol{n}\in\mathcal{N}(V_j)}\prod\limits_{i=1}^{V_j-1}\begin{pmatrix} n_i \\ S^{\mathrm{u}}-\sum_{k=1}^{i-1}n_i \end{pmatrix}$, and, hence, the number of actions for the users over uplink and downlink is $\begin{pmatrix} S^{\mathrm{d}}-1 \\ |\mathcal{N}(V_j)|-1 \end{pmatrix}\sum\limits_{\boldsymbol{n}\in\mathcal{N}(V_j)}\prod\limits_{i=1}^{V_j-1}\begin{pmatrix} n_i \\ S^{\mathrm{u}}-\sum_{k=1}^{i-1}n_i \end{pmatrix}$. This completes the proof.

B. Proof of Theorem 2

In order to prove this theorem, we first need to prove that the ESN-based learning algorithm converges to a constant value. Here, we do not know the exact value to which the proposed algorithm converges. Our purpose is to prove that the proposed algorithm cannot diverge. Then, we derive the exact value to which the ESN converges. For i), based on [23, Theorem 8], the conditions of convergence for an ESN are: a) The ESN is k-step unambiguous and b) The ESN-based learning process is k order Markov decision process (MDP). Here, the definition of k-step unambiguous can be given as follows:

Definition 2. Given an ESN with initial state $\boldsymbol{\mu}_{0,j}$, we assume that the input sequence $\boldsymbol{x}_{0,j},\ldots,\boldsymbol{x}_{\tau,j}$ results in an internal state $\boldsymbol{\mu}_{\tau,j}$, and the input sequence $\boldsymbol{x}'_{0,j},\ldots,\boldsymbol{x}'_{\tau',j}$ results in an internal state $\boldsymbol{\mu}'_{\tau',j}$. If $\boldsymbol{\mu}_{\tau,j}=\boldsymbol{\mu}'_{\tau',j}$ implies that $\boldsymbol{x}_{\tau-i,j}=\boldsymbol{x}'_{\tau'-i,j}$, for all $i=0,\ldots,\tau$, then the ESN is k-step unambiguous.

Here, $\boldsymbol{u}_{\tau,j} = \boldsymbol{u}'_{\tau',j}$ can be rewritten as:

$$\begin{aligned}\boldsymbol{u}_{\tau,j} - \boldsymbol{u}'_{\tau',j} &= \boldsymbol{W}_j \left(\boldsymbol{\mu}_{\tau-1,j} - \boldsymbol{\mu}'_{\tau'-1,j}\right) + \boldsymbol{W}_j^{\text{in}} \left(\boldsymbol{x}_{\tau,j} - \boldsymbol{x}'_{\tau',j}\right) \\ &= \begin{bmatrix} w_{11}\left(\mu_{\tau-1,j1} - \mu'_{\tau'-1,j1}\right) \\ \vdots \\ w_{N_w N_w}\left(\mu_{\tau-1,jN_w} - \mu'_{\tau'-1,jN_w}\right) \end{bmatrix} - \begin{bmatrix} \boldsymbol{W}_{j1}^{\text{in}}\left(\boldsymbol{x}_{\tau,j} - \boldsymbol{x}'_{\tau',j}\right) \\ \vdots \\ \boldsymbol{W}_{jN_w}^{\text{in}}\left(\boldsymbol{x}_{\tau,j} - \boldsymbol{x}'_{\tau',j}\right) \end{bmatrix}, \end{aligned} \tag{19}$$

where $\mu_{\tau-1,jk}$ is element k of $\boldsymbol{\mu}_{\tau-1,j}$ and $\mu'_{\tau'-1,jk}$ element k of $\boldsymbol{\mu}'_{\tau'-1,j}$. Since the tanh function in (16) ranges from -1 to 1, the maximum value of $\left(\mu_{\tau-1,jk} - \mu'_{\tau'-1,jk}\right)$ is 2. As $w_{kk} \in (-1, 1), k = 1, \ldots, N_w$, $\max_k w_{kk}\left(\mu_{\tau-1,jk} - \mu'_{\tau-1,jk}\right) < 2$. In this case, if $\boldsymbol{W}_{jk}^{\text{in}}\left(\boldsymbol{x}_{\tau,j} - \boldsymbol{x}'_{\tau,j}\right) \geq 2$, then $\boldsymbol{\mu}_{\tau,j} - \boldsymbol{\mu}'_{\tau',j} \neq 0$. Therefore, if $\boldsymbol{\mu}_{\tau,j} - \boldsymbol{\mu}'_{\tau',j} = 0$, then $\boldsymbol{\mu}_{\tau-1,j} = \boldsymbol{\mu}'_{\tau'-1,j}$ and $\boldsymbol{x}_{\tau,j} = \boldsymbol{x}'_{\tau',j}$. In this case, an ESN is k-step unambiguous when $\boldsymbol{W}_{ji}^{\text{in}}\left(\boldsymbol{x}_{\tau,j} - \boldsymbol{x}'_{\tau,j}\right) \geq 2$. Since the dynamic reservoir can only store limited ESN information [17], the dynamic reservoir state $\boldsymbol{\mu}_{\tau,j}$ only depends on the finite past reservoir states, i.e., $\boldsymbol{\mu}_{\tau-1,j}, \ldots, \boldsymbol{\mu}_{\tau-k,j}$. Moreover, the number of reservoir states and actions in the proposed algorithm is finite. Therefore, the proposed ESN-based algorithm is a k order MDP and, hence, condition 2) is satisfied. For case 2), if the learning rate of the proposed algorithm satisfies Robbins-Monro conditions and the proposed algorithm is a k order MDP, the proposed algorithm will satisfy the conditions in [25, Theorem 1] and, hence, converges to a region. For both cases i) and ii), based on [25, Theorem 1], the proposed ESN-based learning algorithm will converge to the utility value, $\hat{\boldsymbol{u}}_j$. This completes the proof.

REFERENCES

[1] M. Chen, W. Saad, and C. Yin, "Resource management in a network of wireless virtual reality devices: Machine learning meets multi-attribute utility theory," *submitted to IEEE Global Communications Conference (GLOBECOM)*, December 2017.

[2] P. Rosedale, "Virtual reality: The next disruptor: A new kind of worldwide communication," *IEEE Consumer Electronics Magazine*, vol. 6, no. 1, pp. 48–50, Jan. 2017.

[3] HTC, "Htc vive," https://www.vive.com/us/.

[4] E. Başтuğ, M. Bennis, M. Médard, and M. Debbah, "Towards interconnected virtual reality: Opportunities, challenges and enablers," *arXiv preprint arXiv:1611.05356*, 2016.

[5] F. Qian, L. Ji, B. Han, and V. Gopalakrishnan, "Optimizing 360 video delivery over cellular networks," in *Proc. of All Things Cellular (ATC) Workshop on Operations, Applications and Challenges*, New York, USA, 2016, Oct.

[6] C. Richardt, Y. Pritch, H. Zimmer, and A. Sorkine-Hornung, "Megastereo: Constructing high-resolution stereo panoramas," in *Proc. of the IEEE Conference on Computer Vision and Pattern Recognition*, Portland, OR, USA, June 2013.

[7] S. Sridhar, F. Mueller, M. Zollhöfer, D. Casas, A. Oulasvirta, and C. Theobalt, "Real-time joint tracking of a hand manipulating an object from RGB-D input," in *Proc. of European Conference on Computer Vision*, Amsterdam, Netherlands, Oct. 2016.

[8] A. Rovira and M. Slater, "Reinforcement learning as a tool to make people move to a specific location in immersive virtual reality," *International Journal of Human-Computer Studies*, vol. 98, pp. 89–94, Feb. 2017.

[9] T. Pfeiffer and C. Memili, "Model-based real-time visualization of realistic three-dimensional heat maps for mobile eye tracking and eye tracking in virtual reality," in *Proc. of the Ninth Biennial ACM Symposium on Eye Tracking Research & Applications*, Charleston, South Carolina, Mar. 2016.

[10] L. Musavian and Q. Ni, "Effective capacity maximization with statistical delay and effective energy efficiency requirements," *IEEE Transactions on Wireless Communications*, vol. 14, no. 7, pp. 3824–3835, July 2015.

[11] X. Wu, Y. Tang, and W. Zhang, "Stability analysis of stochastic delayed systems with an application to multi-agent systems," *IEEE Transactions on Automatic Control*, vol. 61, no. 12, pp. 4143–4149, Dec. 2016.

[12] C. She, C. Yang, and T. Q. S. Quek, "Cross-layer transmission design for tactile internet," *available online: arxiv.org/abs/1610.02800*, Oct. 2016.

[13] N. Brahmi, O. N. Yilmaz, K. W. Helmersson, S. A. Ashraf, and J. Torsner, "Deployment strategies for ultra-reliable and low-latency communication in factory automation," in *Proc. of IEEE Global Communications Conference Workshops*, San Diego, CA, USA, Feb. 2015.

[14] P. Kela, M. Costa, J. Salmi, K. Leppanen, J. Turkka, T. Hiltunen, and M. Hronec, "A novel radio frame structure for 5G dense outdoor radio access networks," in *Proc. of IEEE Vehicular Technology Conference (VTC Spring)*, Nanjing, China, May 2015.

[15] A. E. Abbas, "Constructing multiattribute utility functions for decision analysis," *INFORMS Tutorials in Operations Research*, pp. 62–98, Oct. 2010.

[16] M. Chen, M. Mozaffari, W. Saad, C. Yin, M. Debbah, and C. S. Hong, "Caching in the sky: Proactive deployment of cache-enabled unmanned aerial vehicles for optimized quality-of-experience," *IEEE Journal on Selected Areas on Communications (JSAC), Special Issue on Human-In-The-Loop Mobile Networks*, to appear, 2017.

[17] H. Jaeger, "Short term memory in echo state networks," in *GMD Report*, 2001.

[18] R. Ali and T. Peter, "Minimum complexity echo state network," *IEEE Transactions on Neural Networks*, vol. 22, no. 1, pp. 131–144, November 2011.

[19] R. A. Earnshaw, *Virtual Reality Systems*, Academic press, 2014.

[20] A. Zhu, P. J. Draxler, C. Hsia, T. J. Brazil, D. F. Kimball, and P. M. Asbeck, "Digital predistortion for envelope-tracking power amplifiers using decomposed piecewise volterra series," *IEEE Transactions on Microwave Theory and Techniques*, vol. 56, no. 10, pp. 2237–2247, Oct. 2008.

[21] G. C. Burdea and P. Coiffet, *Virtual Reality Technology*, John Wiley & Sons, 2003.

[22] Z. Han, D. Niyato, W. Saad, T. Basar, and A. HjÃ¸rungnes, *Game Theory in Wireless and Communication Networks: Theory, Models, and Applications*, Cambridge University Press, 2012.

[23] I. Szita, V. Gyenes, and A. Lőrincz, "Reinforcement learning with echo state networks," *Lecture Notes in Computer Science*, vol. 4131, pp. 830–839, 2006.

[24] R. Sutton and A. Barto, *Reinforcement Learning:An Introduction*, MIT Press, 1998.

[25] M. Chen, W. Saad, and C. Yin, "Echo state networks for self-organizing resource allocation in LTE-U with uplink-downlink decoupling," *IEEE Transactions on Wireless Communications*, vol. 16, no. 1, January 2017.

[26] M. Chen, W. Saad, C. Yin, and M. Debbah, "Echo state networks for proactive caching in cloud-based radio access networks with mobile users," *available online: arxiv.org/abs/1607.00773*, July 2016.

[27] Oculus, "Mobile VR Media Overview," https://developer3.oculus.com/documentation/mobilesdk/latest/concepts/mobile-media-overview/.

[28] M. Bennis, S.M. Perlaza, P. Blasco, Z. Han, and H.V. Poor, "Self-organization in small cell networks: A reinforcement learning approach," *IEEE Transactions on Wireless Communications*, vol. 12, no. 7, pp. 3202–3212, June 2013.

[29] F. Kelly, "Charging and rate control for elastic traffic," *European Transactions on Telecommunications*, vol. 8, no. 1, pp. 33–37, 1997.

[30] M. Bennis and D. Niyato, "A Q-learning based approach to interference avoidance in self-organized femtocell networks," in *Proc. of IEEE Global Commun. Conference (GLOBECOM) Workshop on Femtocell Networks*, Miami, FL, USA, Dec. 2010.

[31] M. Abrash, "What VR could, should, and almost certainly will be within two years," https://media.steampowered.com/apps/abrashblog/Abrash%20Dev%20Days%202014.pdf.